doi:10.1038/nature12479

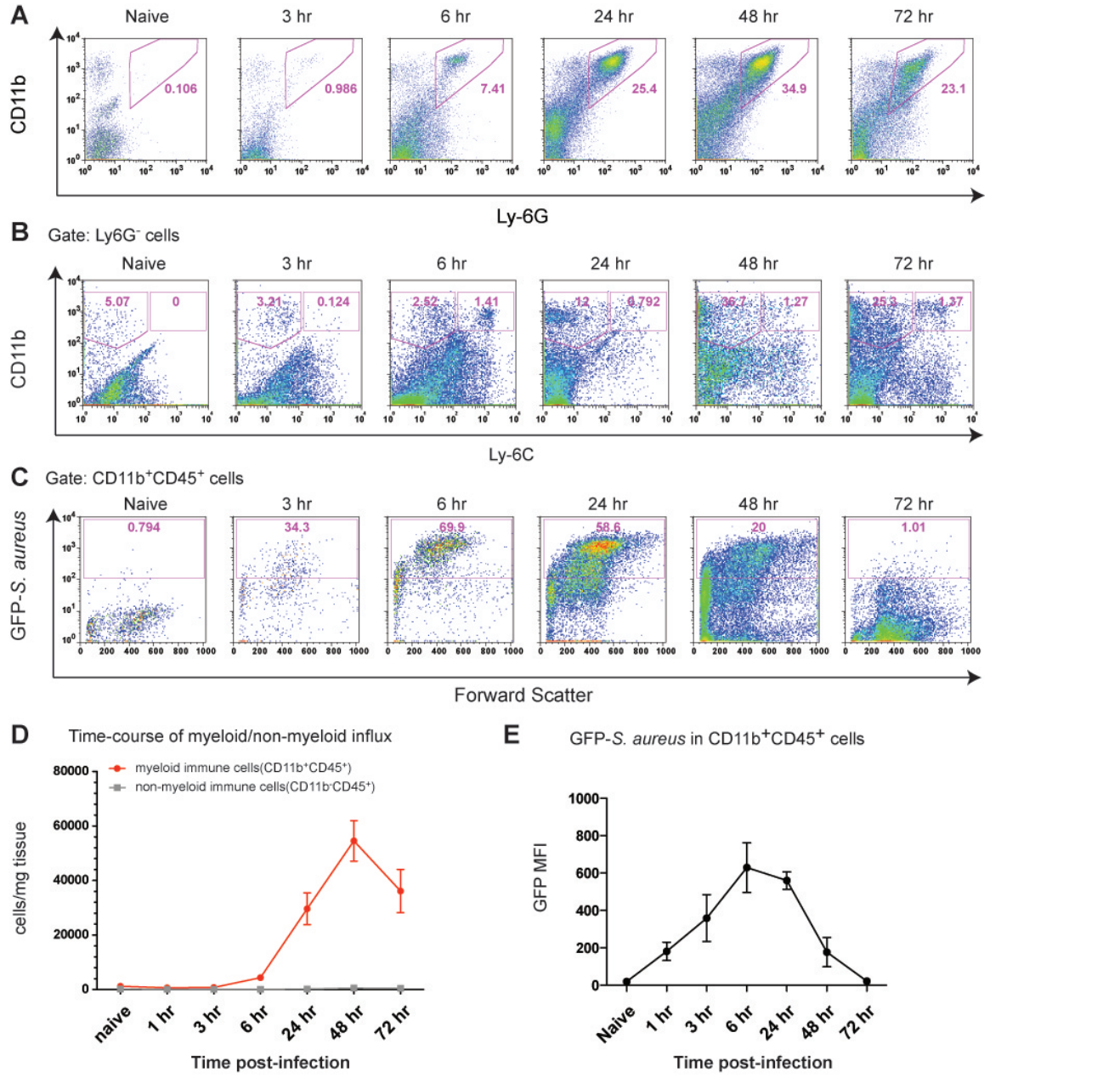

Supplementary Figure 1. Kinetics of immune cell influx in *S. aureus* infected paw tissue and myeloid cell ingestion of bacteria. **(A)** Flow cytometry of $CD11b^{+}Ly6G^{+}$ neutrophils (gates shown) in plantar tissues post- *S. aureus* infection. **(B)** After gating out $CD11b^{+}Ly6G^{+}$ cells, $CD11b^{+}Ly6C^{hi}$ and $CD11b^{+}Ly6C^{lo}$ monocytes/macrophages were analyzed during infection (left and right gates, respectively). **(C)** Mice were infected with GFP-*S. aureus* ($5x10^{6}$ c.f.u.): flow cytometry shows GFP within myeloid cells ($CD11b^{+}CD45^{+}$), possibly reflecting ingestion of *S. aureus* at different time-points. **(D)** Determination of myeloid and non-myeloid immune cells in infected tissues shows myeloid cell peak at 48 h. n=3 samples/time-point. **(E)** GFP-*S. aureus* mean fluorescence intensity (MFI, geometric mean) within myeloid cells peak at 6 h. n=3 samples/time-point. Error bars, mean±s.e.m.

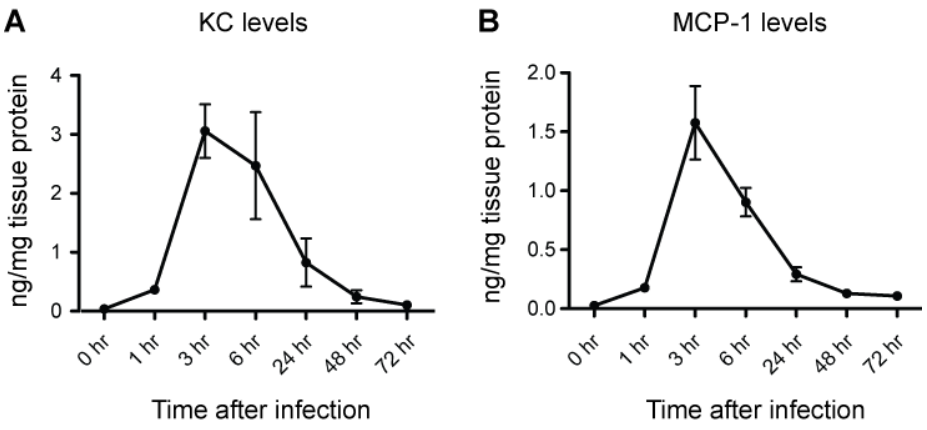

Supplementary Figure 2. Time-course of KC and MCP-1 levels in *S. aureus* infected tissues. Plantar paw tissue was isolated following infection with $5x10^6$ c.f.u. *S. aureus*, homogenized and analyzed for levels of **(A)** KC (Cxcl1) and **(B)** MCP-1 at different time-points using Luminex mouse cytokine beads. n=4 biological samples/time-point. Values are normalized to total plantar tissue protein levels as measured by BCA assay. Error bars, mean±s.e.m.

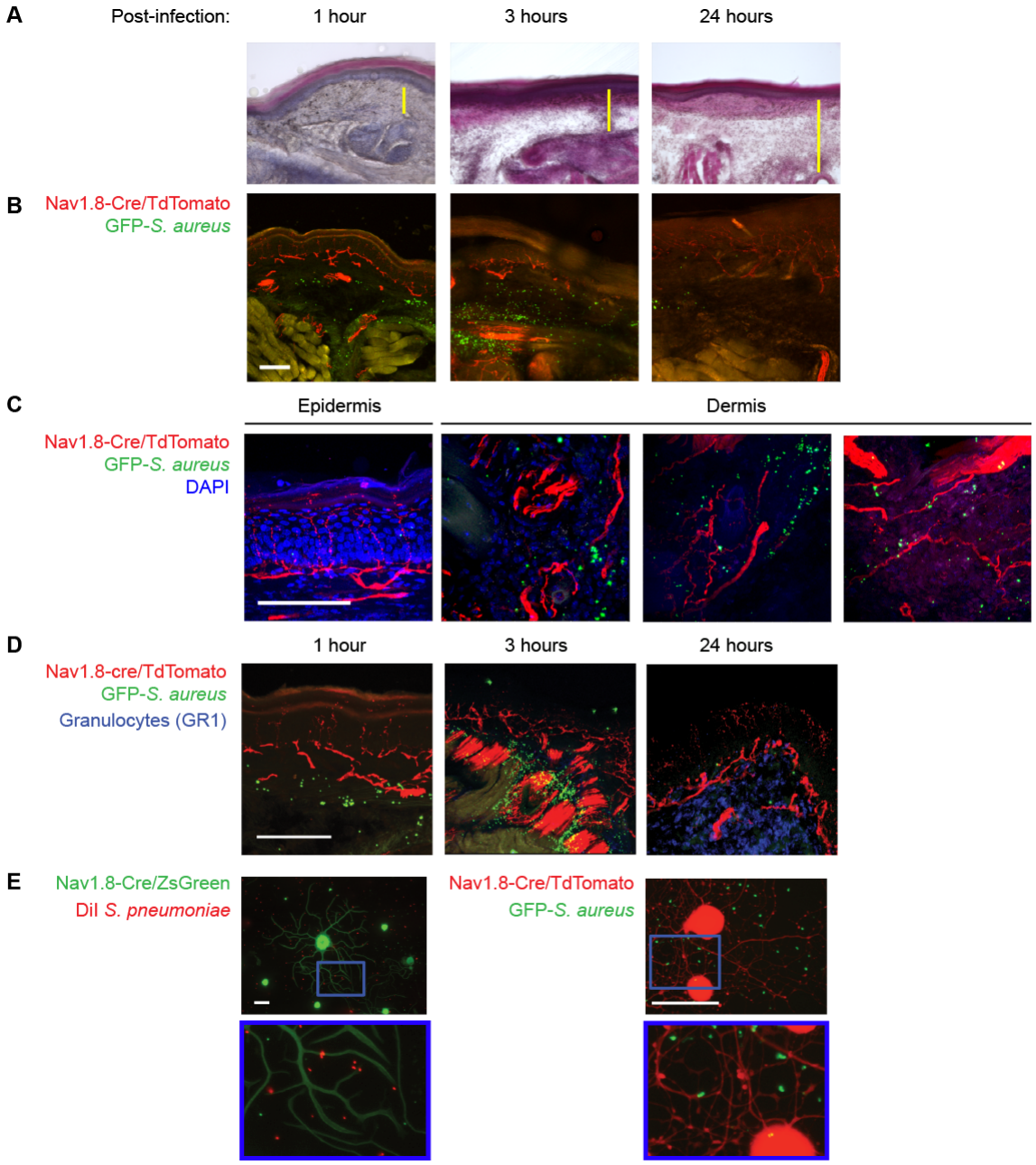

Supplementary Figure 3. Bacteria localize in proximity with nociceptor nerve fibres in infected tissues and neurites in co-cultures. (A) Haematoxylin/Eosin staining shows tissue swelling between muscle and skin layers post-*S. aureus* infection (yellow lines). **(B)** Time-course of GFP-USA300 accumulation in Nav1.8-Cre/TdTomato plantar tissue post-infection. **(C)** GFP-USA300 (green) were often juxtaposed to TdTomato nerve fibres (red) in dermal but not epidermal regions, 3 h post-infection. **(D)** Anti-GR1 staining shows granulocytes appearing and fewer numbers of GFP-USA300 by 24 h post-infection. **(E)** Nav1.8-Cre/ZsGreen or Nav1.8-Cre/TdTomato DRG neurons were co-cultured with CMTMR-*S. pneumoniae* (10^7 c.f.u., heat-killed) or live GFP-USA300 (*S. aureus,* 10^7 c.f.u.). Cultures were fixed and imaged by fluorescence microscopy. Bacteria were often in proximity to neurites. Scale bars, 100 µm.

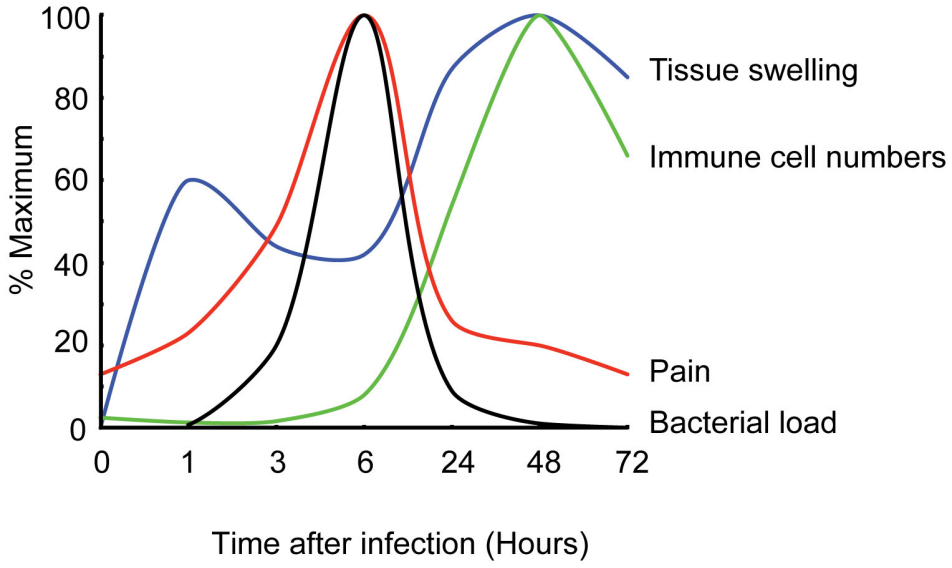

Supplementary Figure 4. Time-course of tissue swelling, immune cell accumulation, pain and bacterial load following *S. aureus* infection.
Each parameter was normalized to the maximum and connected by smoothened extrapolation. For the pain parameter, mechanical Von Frey thresholds were converted to inverse values. Pain correlates strongly with live bacterial load, and not immune cell numbers or tissue swelling.

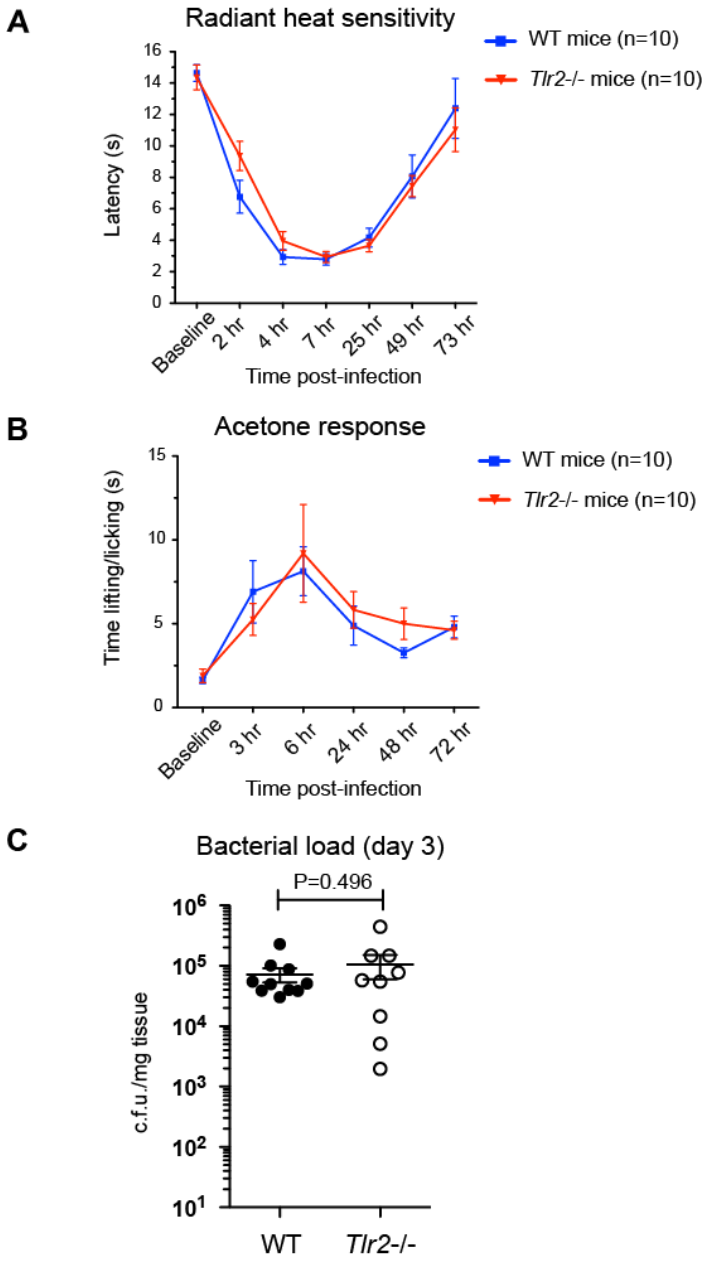

Supplementary Figure 5. ***Tlr2*** **deficiency does not contribute to** ***S. aureus*** **induced heat or cold hypersensitivity.**
(A-B) Mice infected with 5x10^6 c.f.u. *S. aureus* were tested for heat sensitivity (Hargreave's radiant heat test) and acetone response sensitivity. *Tlr2*$^{-/-}$ and WT controls follow a similar time-course in the induction and resolution of hyperalgesia. **(C)** Bacterial load of *S. aureus* in *Tlr2*$^{-/-}$ and WT control paw tissue show similar levels at 73 h post-infection (P-value, t-test). Error bars, mean±s.e.m.

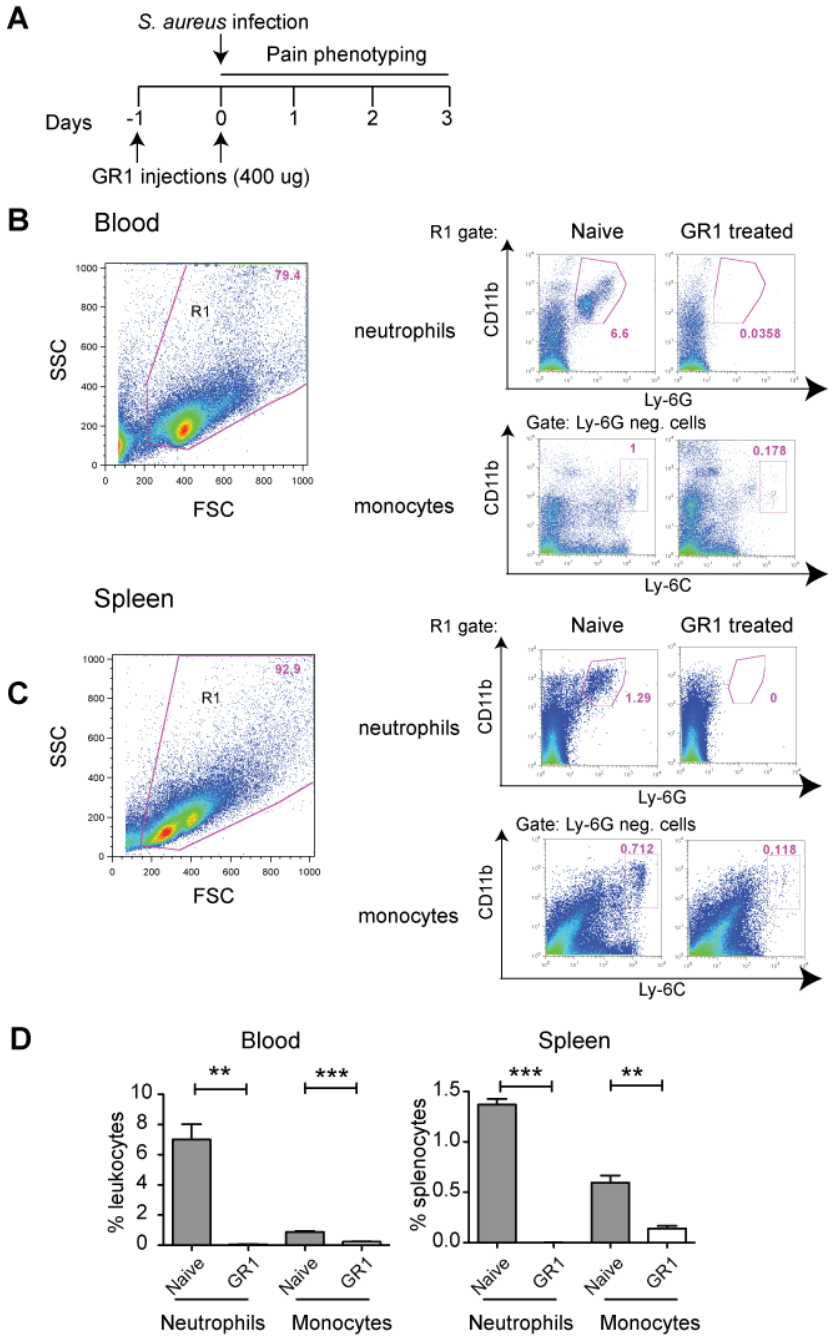

Supplementary Figure 6. GR1 antibody treatment eliminates blood-borne and splenic neutrophils, monocytes. (A) Injection scheme for GR1 treatment: 400 µg of GR1 or control rat IgG antibody was injected i.p. 24 h and one hour before live *S. aureus* infection. **(B-C)** Flow cytometry of blood cells and splenic cells from untreated mice or mice treated with GR1 at 24 h post-treatment. CD11b, Ly6G, Ly6C staining shows depletion of the neutrophil ($CD11b^{+}Ly6G^{+}$), monocyte ($CD11b^{+}Ly6G^{-}Ly6C^{+}$) populations. **(D)** Quantification of populations analyzed in B-C, showing significant depletion of blood and splenic neutrophil/monocytes (n=3 mice/group, **, P<0.01; ***, P<0.001, t-test). Error bars, mean±s.e.m.

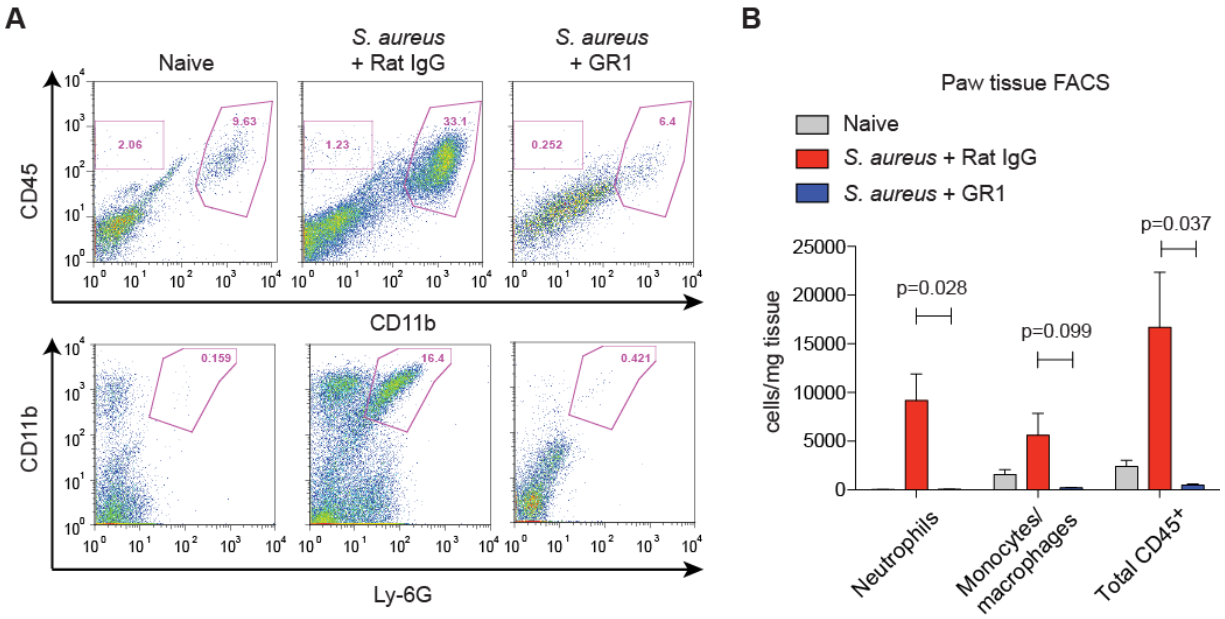

Supplementary Figure 7. GR1 treatment eliminates tissue infiltrating neutrophils and monocytes during *S. aureus* infection.

400 μg of GR1 or control rat IgG was injected i.p. 24 h and one hour prior to intraplantar infection with LAC/USA300 ($5x10^6$ c.f.u.) **(A)** Representative flow cytometry plots of infected plantar tissue shows depletion of myeloid immune cells ($CD11b^+CD45^+$) and neutrophils ($CD11b^+Ly6G^+$) at 24 h after *S. aureus* infection. **(B)** Quantification of plantar tissue neutrophil ($CD11b^+Ly6G^+$), monocytes/macrophages ($CD11b^+Ly6G^-Ly6C^+$), and total immune cells quantified using the pan-immune marker, CD45, 24 h post- *S. aureus* infection (P-value, t-test). Error bars, mean±s.e.m.

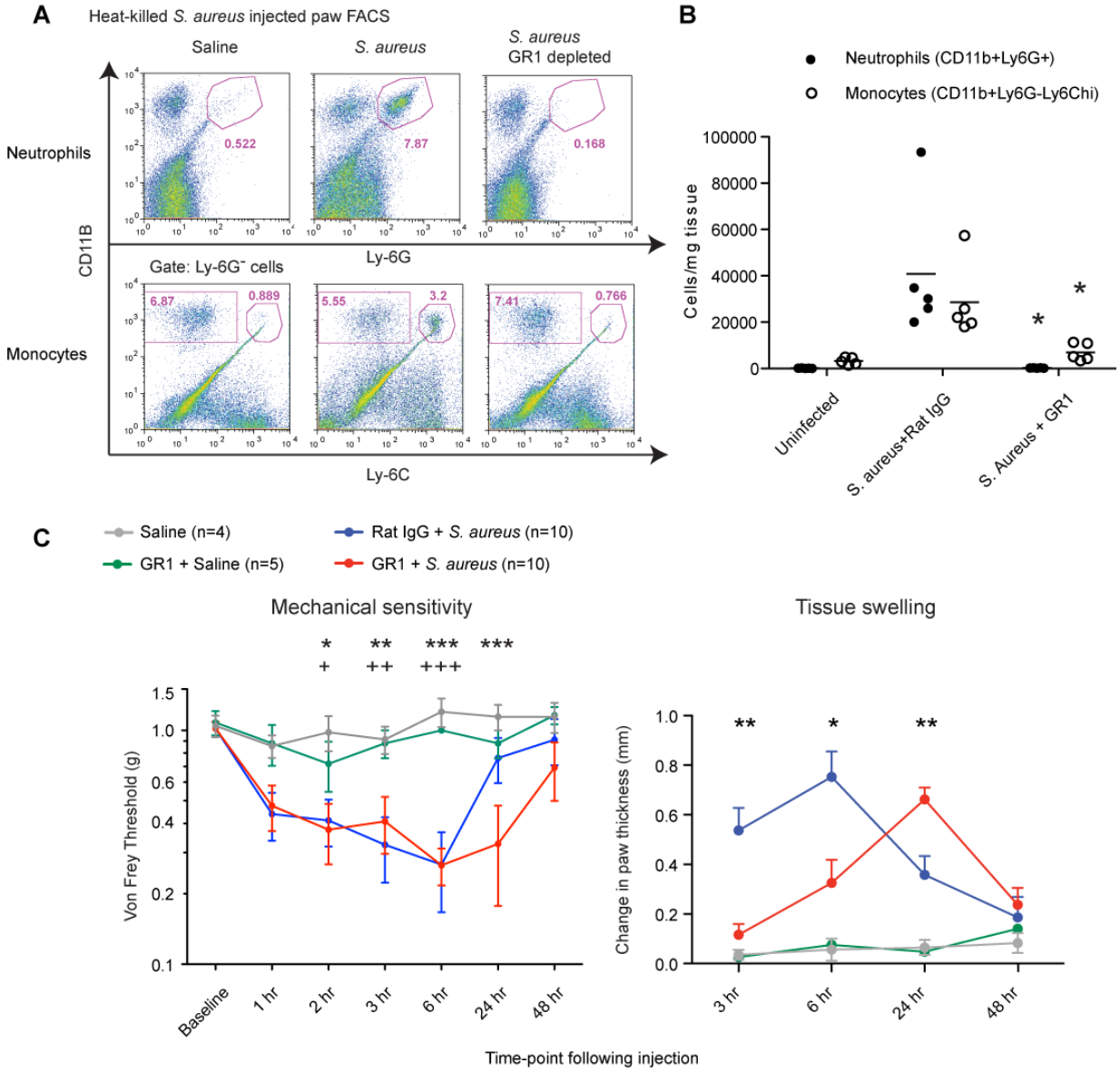

Supplementary Figure 8. GR1 treatment does not decrease pain caused by heat-killed (hk) *S. aureus*. Hk-*S. aureus* (10^8 c.f.u.) was injected into the hind-paw: tissue swelling, plantar immune cell populations, and mechanical hypersensitivity were measured. Unlike live infection, hk-*S. aureus* induced Ly6C^{hi} monocytes rather than Ly6C^{lo} monocytes. Pain correlated with tissue swelling (vs. Fig. 1a). **(A-B)** GR1 or rat IgG (400 µg) was injected i.p. 24 h and one hour prior to hk-*S. aureus*. Flow cytometry shows significant decreases in neutrophils, monocytes in plantar tissues 48 hr post-GR1 injection (5 mice/group; *, P<0.05, t-test, GR1 vs. rat IgG). **(C)** Mechanical hyperalgesia was similar in GR1 and rat IgG treated mice injected with hk-*S. aureus*. (Bonferroni, *, P<0.05; **, P<0.01; ***, P<0.001 GR1 and hk *S.a.* vs. saline; +, P<0.05; ++, P<0.01; +++, P<0.001 Rat IgG and hk *S.a.* vs. saline). GR1 treatment significantly decreased swelling at 3 h, 6 h, and caused more swelling at 24 h relative to rat IgG treated mice (Two-way ANOVA with Bonferroni, *, P<0.05; **, P<0.01). Thus, GR1 treatment affects tissue swelling but not mechanical pain following hk-*S. aureus* injection. Error bars, mean±s.e.m.

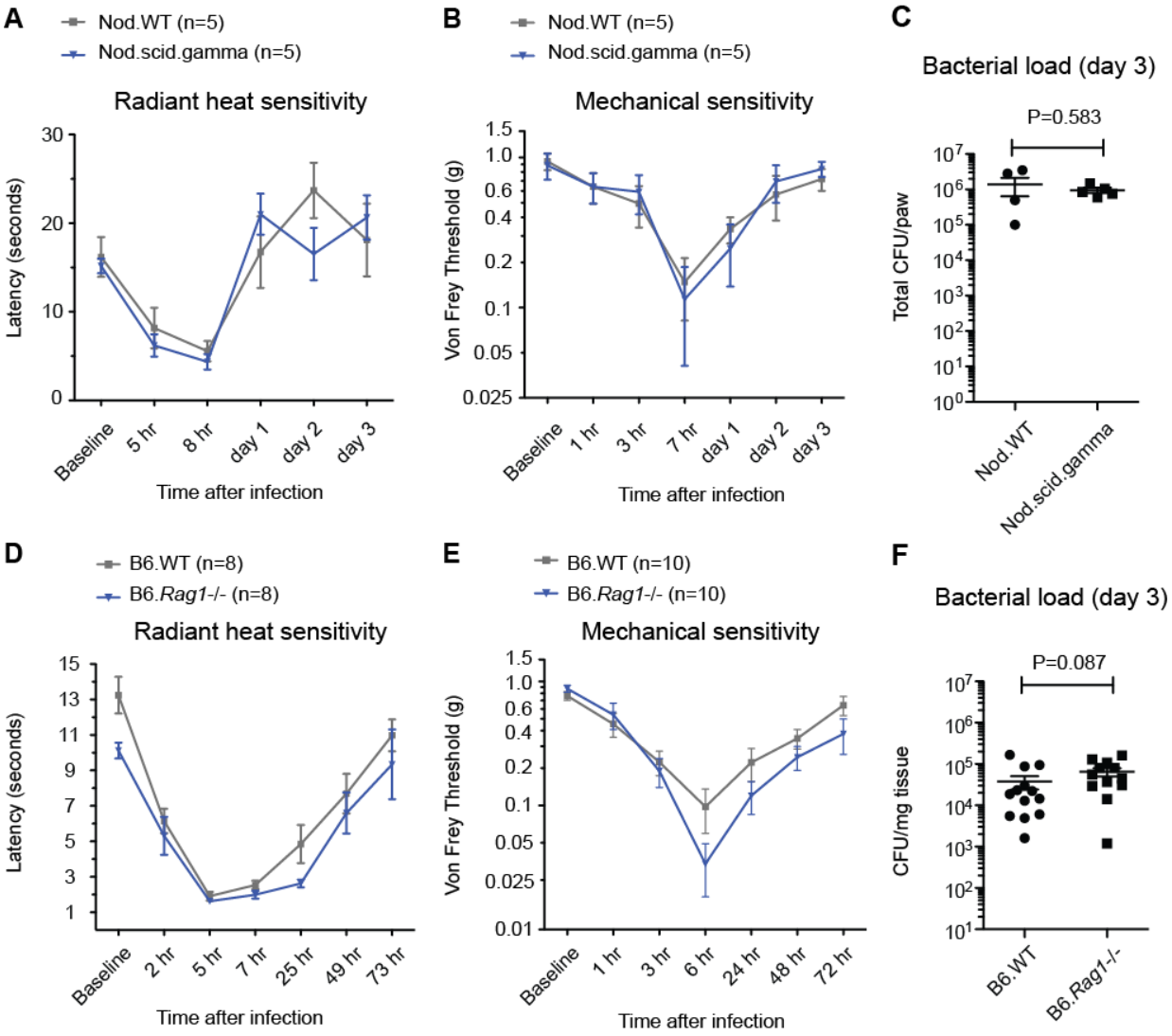

Supplementary Figure 9. Heat and mechanical hypersensitivity are not reduced in Nod.scid.gamma or B6.*Rag1*-/- mice following *S. aureus* infection.
In **A-C**, Nod.scid.gamma and Nod.WT mice, and in **D-F,** B6.*Rag1*$^{-/-}$ mice and B6.WT mice were tested for pain-like sensitivity following *S. aureus* infection (5x10^6 c.f.u. LAC). **(A-B)** No significant differences in heat hypersensitivity (P=0.314, Two-way RM ANOVA) were observed between infected Nod.scid.gamma and Nod.WT mice, or mechanical hypersensitivity (P=0.908, Two-way RM ANOVA). **(C)** *S. aureus* bacterial load did not differ significantly 3 days following infection (P=0.583, t-test, Nod.scid.gamma, n=5; Nod.WT, n=5) note: one Nod.WT sample was 0 c.f.u., so not displayed on axis). Behavioral analysis of the Nod mouse strain was challenging because of baseline hyperactivity despite repeated habituations. **(D-E)** No significant differences in heat (P=0.715, Two-way RM ANOVA) or mechanical hypersensitivity (P=0.198, Two-way RM ANOVA) were observed between *S. aureus* infected B6.*Rag1*$^{-/-}$ and B6.WT mice. **(F)** Bacterial load was slightly but not significantly increased in B6.*Rag1*$^{-/-}$ mice compared to B6.WT mice day 3 after *S. aureus* infection (P=0.087, t-test; B6.*Rag1*$^{-/-}$, n=12; B6.WT, n=13). Error bars, mean±s.e.m.

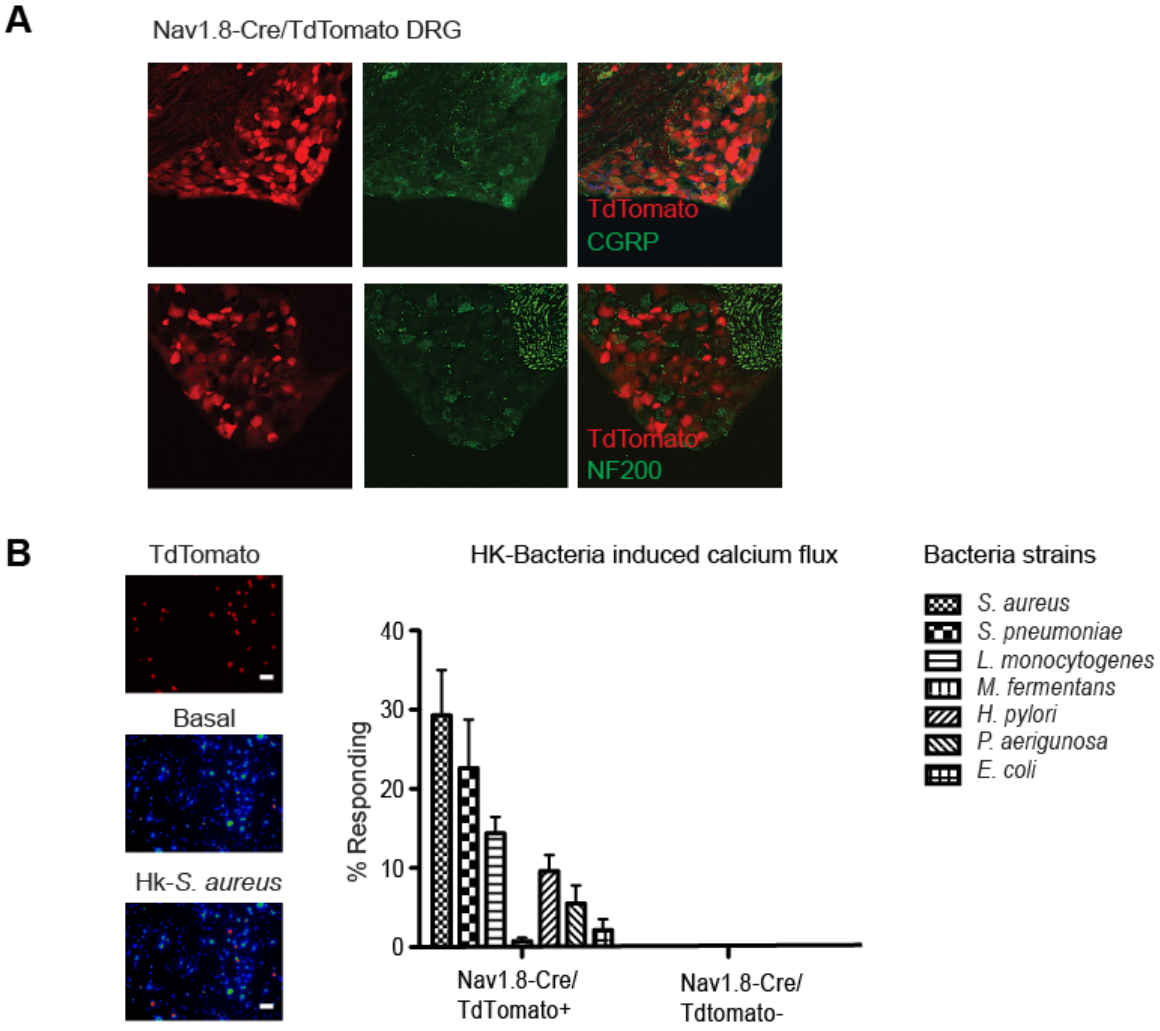

Supplementary Figure 10. Heat-killed bacteria induce calcium flux in Nav1.8 lineage neurons and not other DRG neurons.
(A) Nav1.8-Cre mice were bred with TdTomato reporter mice to generate Nav1.8-Cre/TdTomato mice to mark nociceptor lineage neurons. Lumbar DRG sections were immunostained for CGRP (millipore, 1:1000, green) and neurofilament-200 (Sigma, 1:1000, green). $CGRP^+$ peptidergic neurons were within the Nav1.8-Cre/TdTomato subset, while most $NF200^+$ A-fibers were excluded from the Nav1.8-Cre/TdTomato subset. **(B)** Representative calcium imaging field of TdTomato expressing neurons, with cells before (basal) and after application of hk-*S. aureus*. All *S. aureus* responding neurons were also $TdTomato^+$. Bar graph shows quantification of Nav1.8-Cre/$TdTomato^+$ and Nav1.8-Cre/$TdTomato^-$ DRG neurons responding to different hk-bacteria strains (10^7 c.f.u./ml). Shown are proportions of responding DRG neurons within each Tdtomato subset/field. Error bars, mean±s.e.m.

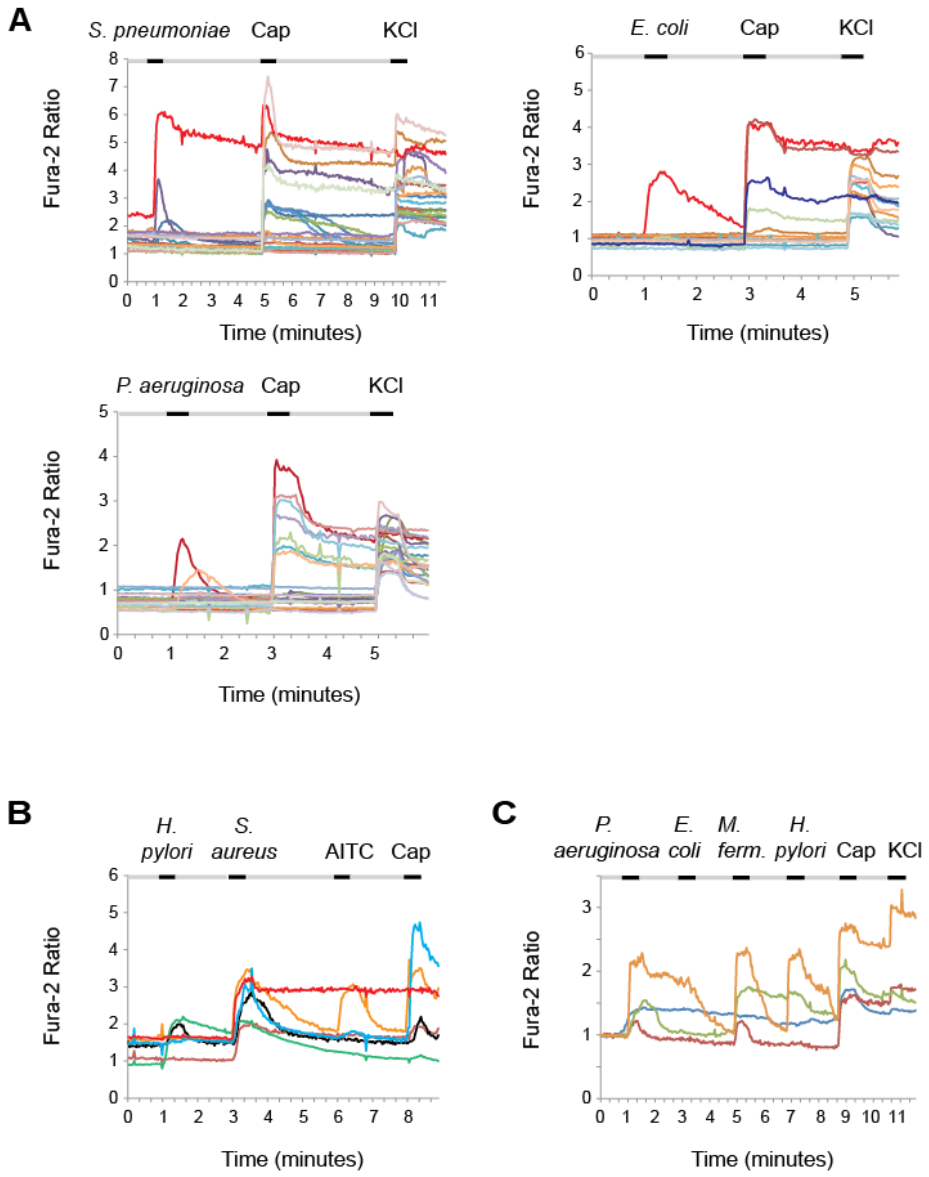

Supplementary Figure 11. Heat-killed bacteria strains induce differential activation of nociceptor subsets.
All heat-killed bacteria were applied at 10^7 c.f.u./ml. **(A)** Sequential application (black) with buffer washout (gray) of hk-*S. pneumoniae*, capsaicin (1 µM), KCl (40 mM) induces activation of a subset of capsaicin responsive DRG neurons (representative ratiometric traces shown). Neuronal responses to hk-*E. coli* and hk-*P. aeruginosa* are also shown. **(B)** DRG neurons subjected to sequential application and washout of hk-*H. pylori*, hk-*S. aureus*, allyl isothiocyanate (AITC, 100 µM), and capsaicin (1 µM). Representative calcium traces show neurons responding hk-*S. aureus* but not to hk-*H. pylori*. **(C)** Sequential application and washout of hk-*P. aerigunosa*, hk-*E. coli,* hk-*M. fermentans,* hk-*H. pylori*, capsaicin (1 µM), and KCL (40 mM) shows representative traces of neurons responding to some bacteria, but not others.

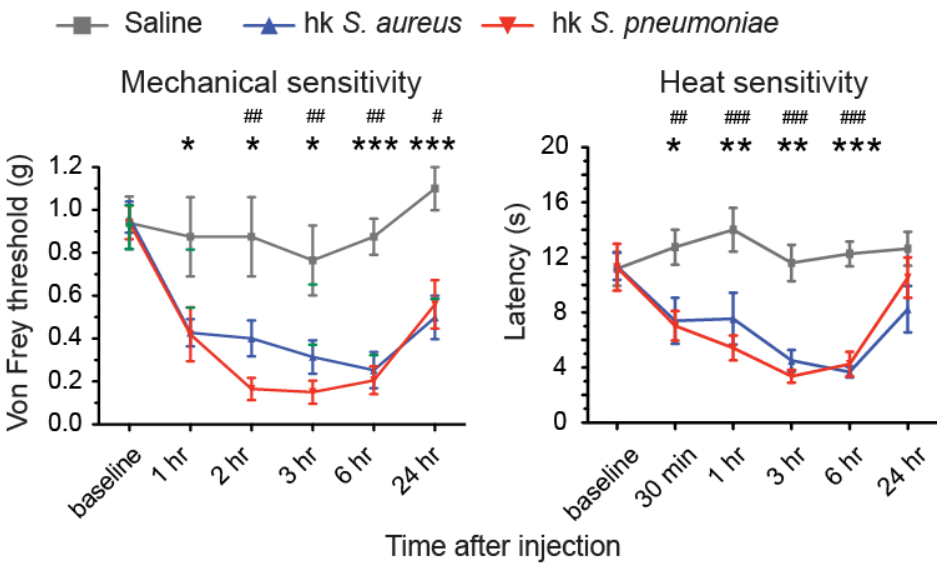

Supplementary Figure 12. Heat-killed *S. aureus* and *S. pneumoniae* injection induces sustained mechanical and heat hypersensitivity.
Left, Mechanical hypersensitivity is induced following injection of 10^8 c.f.u. hk-*S. pneumoniae* (n=6; P=0.0217, Two-way RM ANOVA) or 10^8 c.f.u. hk-*S. aureus* (n=16; P=0.0016, Two-way RM ANOVA) compared with saline injected mice (n=8). Heat hypersensitivity is induced following injection of 10^8 c.f.u. hk-*S. pneumoniae* (n=7, P=0.0005, Two-way RM ANOVA), or 10^8 c.f.u. hk-*S. aureus* (n=7, P=0.026, Two-way RM ANOVA) vs. saline (n=6). Bonferroni post-tests: hk-*S. aureus* vs. saline, #P<0.05; ##P<0.01; ###P<0.001. hk-*S. pneumonia* vs. saline, *P<0.05, **P<0.01, ***P<0.001. Error bars, mean±s.e.m.

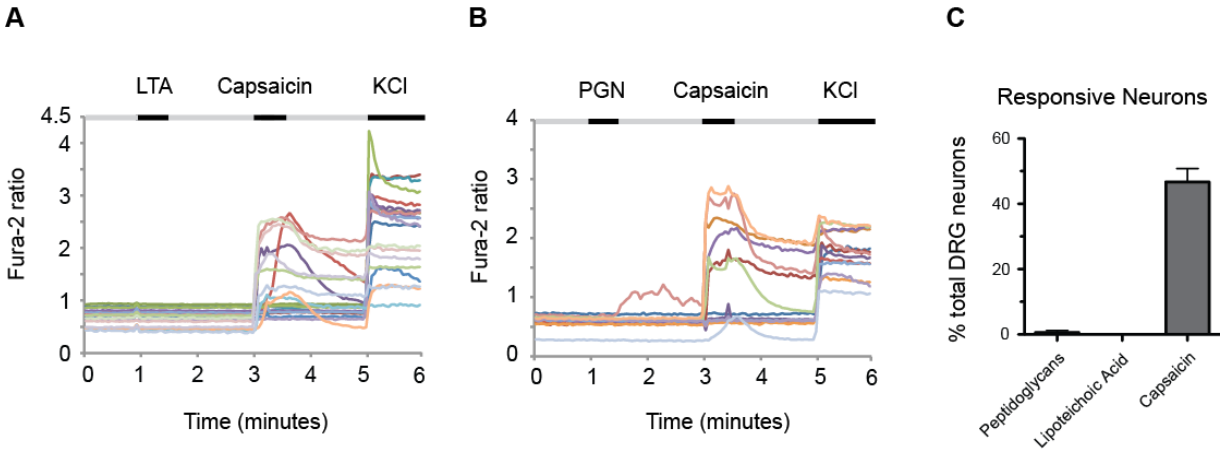

Supplementary Figure 13. *S. aureus* derived LTA and PGN do not induce significant calcium flux in DRG neurons.
Sequential application (black) and buffer washout (gray) of *S. aureus* derived lipoteichoic acid (LTA, 1 µg/mL), *S. aureus* derived peptidoglycan (PGN, 1 µg/mL), capsaicin (1 µM) and KCl (40 mM) shows DRG neurons responding to capsaicin but not to LTA or PGN. **(A-B)** Representative Fura-2 Ca^{2+} ratiometric traces in fields of neurons for PGN, or LTA, followed by capsaicin and KCl. **(C)** Quantification of proportions of DRG neurons responding to PGN, LTA, or Capsaicin out of total KCl responsive neurons. Error bars, mean± s.e.m.

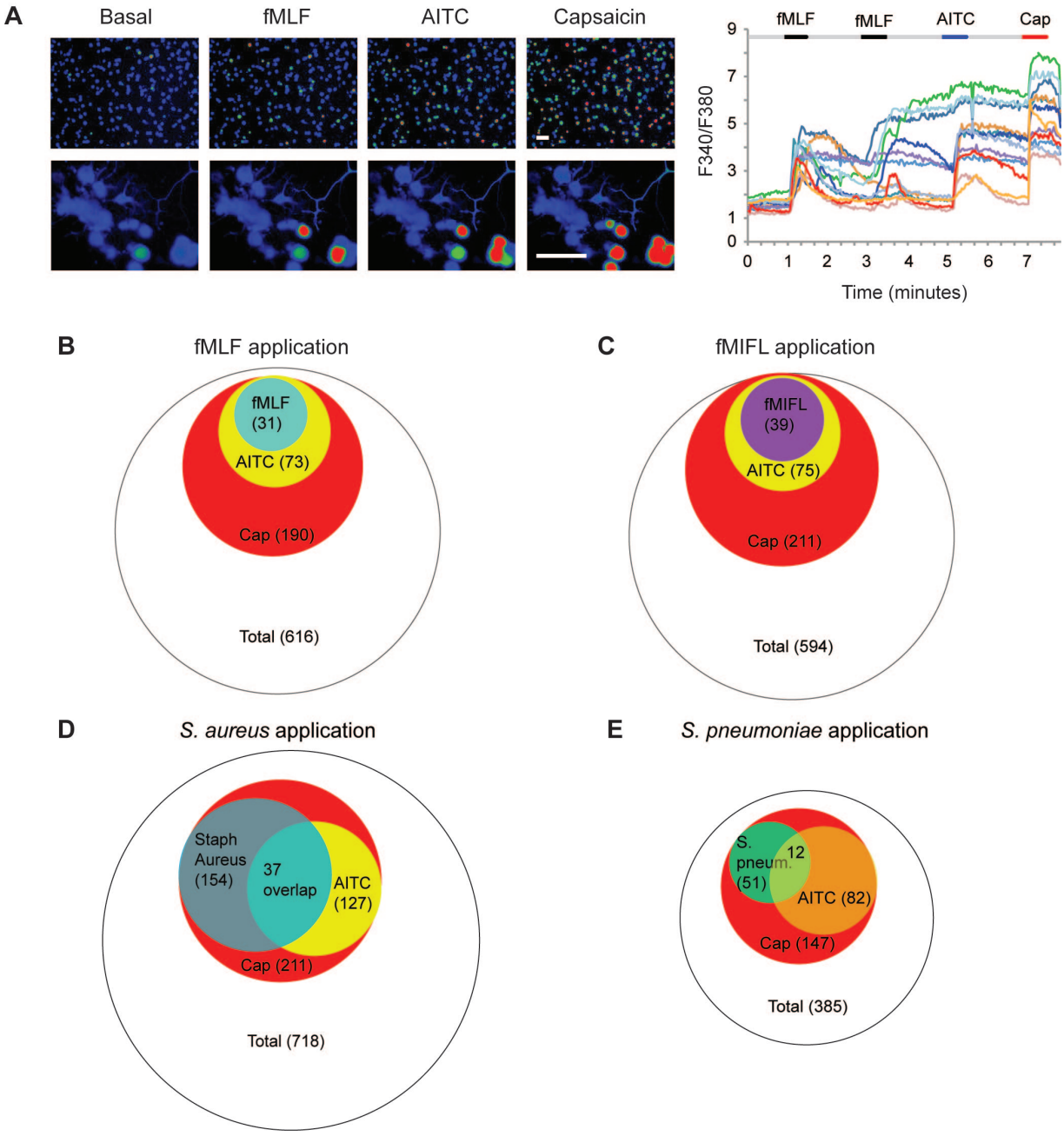

Supplementary Figure 14. Formyl peptides activate a subset of AITC responsive neurons, while heat-killed bacteria activate a larger DRG neuron subset.
(A) Low and high magnification of Fura-2 ratiometric images of DRG neurons after application of fMLF (1 μM), allyl isothiocyanate (AITC, 100 μM), and capsaicin (1 μM). Representative Fura-2 traces are shown at right. Scale bars, 100 μm. **(B-C)** Venn diagrams of DRG neuronal responsive cells, showing that all neurons responding to N-formylated peptides fMLF or fMIFL are also AITC, capsaicin responsive. **(D-E)** Venn diagrams show neurons responding to hk-*S. aureus* or hk-*S. pneumoniae*, indicating that hk-bacteria induce a larger subset of neuronal responses than formylated peptides.

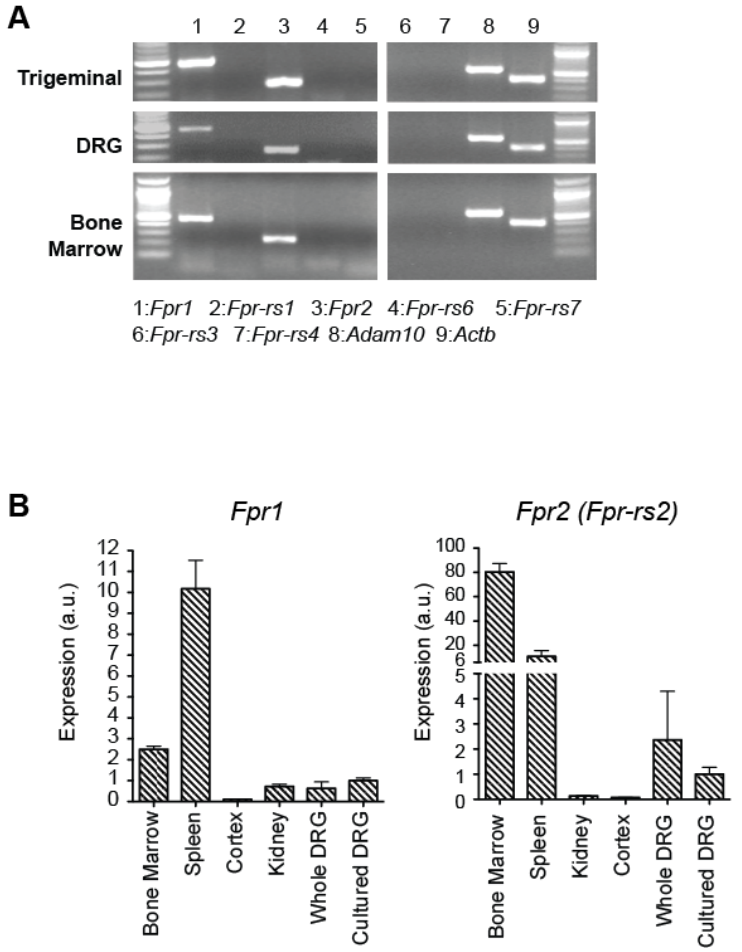

Supplementary Figure 15. *Fpr1* and *Fpr2* but not other Fpr genes are expressed in sensory ganglia.
(A) RT-PCR of *Fpr1, Fpr-rs1, Fpr2 (Fpr-rs2), Fpr-rs6, Fpr-rs7, Fpr-rs3, Fpr-rs4, Adam10, Actb* from cDNA synthesized from mouse trigeminal ganglia, dorsal root ganglia, and bone marrow RNA. *Fpr1, Fpr2*, *Adam10* gene expression were detected, but not other Fpr genes. **(B)** Quantitative PCR for Fpr1 and Fpr2 from mouse bone marrow, spleen, cortex, kidney, whole DRG and cultured DRG neuron-derived cDNA. Fpr1 and Fpr2 are expressed in immune organs (bone marrow, spleen) and DRG. Error bars, mean±s.e.m.

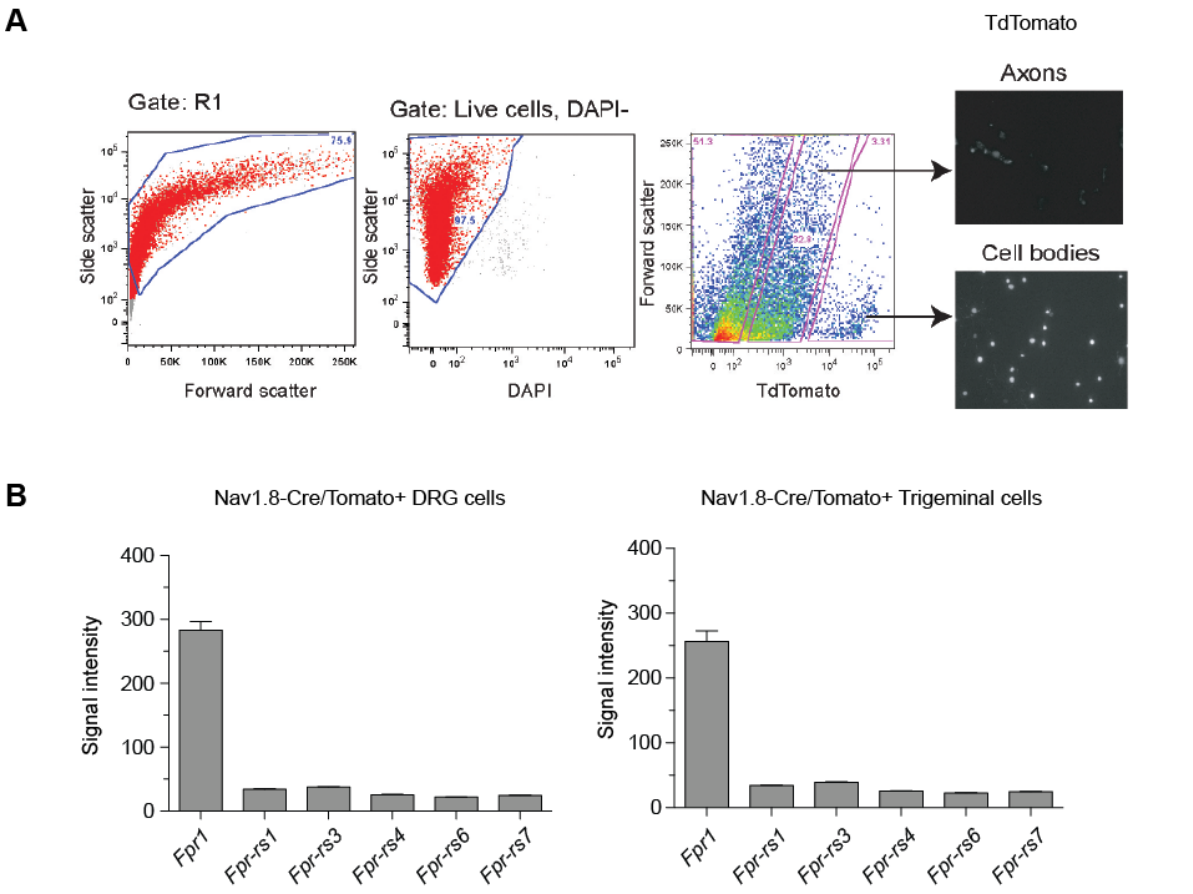

Supplementary Figure 16. FACS purified Nav1.8-Cre/TdTomato$^+$ neurons express *Fpr1*.
(A) DRG from adult Nav1.8-Cre/TdTomato mice were dissected, dissociated, and fluorescence activated cell sorting (FACS) purified: shown is gating strategy for live DRG cells by exclusion of DAPI$^+$ cells followed by gating on neuronal cell bodies, which harbored high Tdtomato$^+$ fluorescence, instead of axons, which harbored low Tdtomato$^+$ fluorescence. Following sorting of cell bodies, neurons were found to be highly pure by microscopy. **(B)** RNA from FACS purified Nav1.8-Cre/TdTomato$^+$ DRG neurons (n=3 samples) and Nav1.8-Cre/TdTomato$^+$ trigeminal neurons (n=4 samples) were subject to microarray analysis. Normalized expression signal intensities are given for *Fpr1* (probeset 10448127), *Fpr-rs1* (probeset 10442098), *Fpr-rs3* (probeset 10448168), *Fpr-rs4* (probeset 10442104), *Fpr-rs6* (probeset 10448148), and Fpr-rs7 (probeset 10448146). Error bars, mean±s.e.m.
Note: The *Fpr2* (*Fpr-rs2*) probeset was not available on this genechip (Affymetrix Mouse Gene ST 1.0), so we do not conclude its presence or absence in sorted Nav1.8-Cre/TdTomato$^+$ neurons.

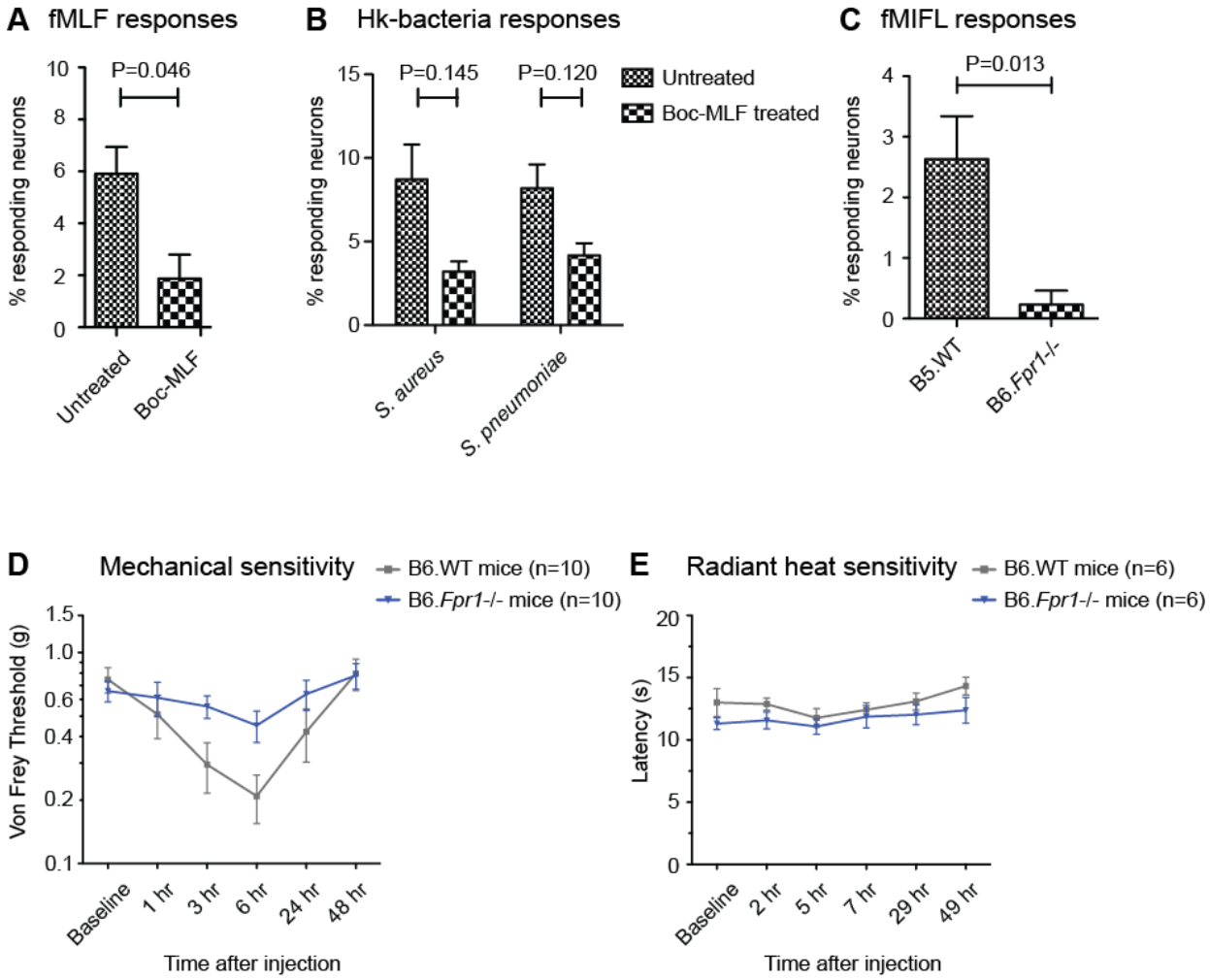

Supplementary Figure 17. FPR1 mediates nociceptor responses to fMIFL and induction of hyperalgesia following fMIFL injection.
(A-B) DRG neurons were treated with buffer alone or with FPR1 antagonist Boc-MLF (10 μM) for 10 minutes prior to application of fMLF (1 μM), hk-*S. aureus* (10^7 c.f.u./ml) or hk-*S. pneumoniae* (10^7 c.f.u./ml). Fura-2 ratiometric imaging determined neurons responding by calcium flux. Boc-MLF decreases the proportion of neurons responding to fMIFL and hk-bacteria (p-value, t-test). **(C)** DRG neurons from B6.WT and B6.*Fpr1*-/- mice were analyzed in parallel for calcium flux responses to fMIFL (1 μM) by Fura-2 ratiometric imaging. The proportion of fMIFL is significantly decreased in *Fpr1*$^{-/-}$ cultures (P-value, t-test). **(D-E)** fMIFL induced mechanical hypersensitivity is significantly reduced in *Fpr1*$^{-/-}$ mice. Following injection of fMIFL (2 nmoles), mechanical hypersensitivity was significantly reduced in *Fpr1*$^{-/-}$ compared to WT mice (P=0.044, Two-way RM ANOVA). Radiant heat sensitivity was not changed by fMIFL injection in both B6.*Fpr1*$^{-/-}$ and B6.WT mice. Error bars, mean±s.e.m.

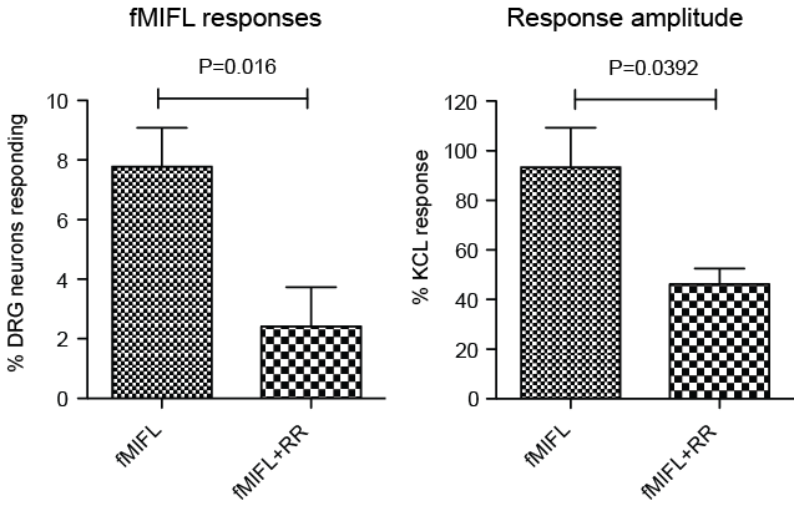

Supplementary Figure 18. Ruthenium Red significantly reduces the proportion and amplitude of fMIFL neuronal responses.
fMIFL (1 μM) was applied to cultured DRG neurons in the presence or absence of Ruthenium Red (RR, 10 μM), and calcium flux responses quantified by Fura-2 ratiometric imaging. **(A)** The proportion of neurons responding to fMIFL by calcium flux is significantly decreased in the presence of RR (P-value, t-test). Out of total DRG neurons, 18/184 responded to fMIFL by calcium flux, while 9/212 responded to fMIFL+RR. **(B)** The amplitude of fMIFL induced calcium flux (Fura-2 ratio) was normalized to the peak response to KCl (40 mM). In the presence of Ruthenium Red, fMIFL response amplitudes were significantly decreased. P-value, t-test. Error bars, mean±s.e.m.

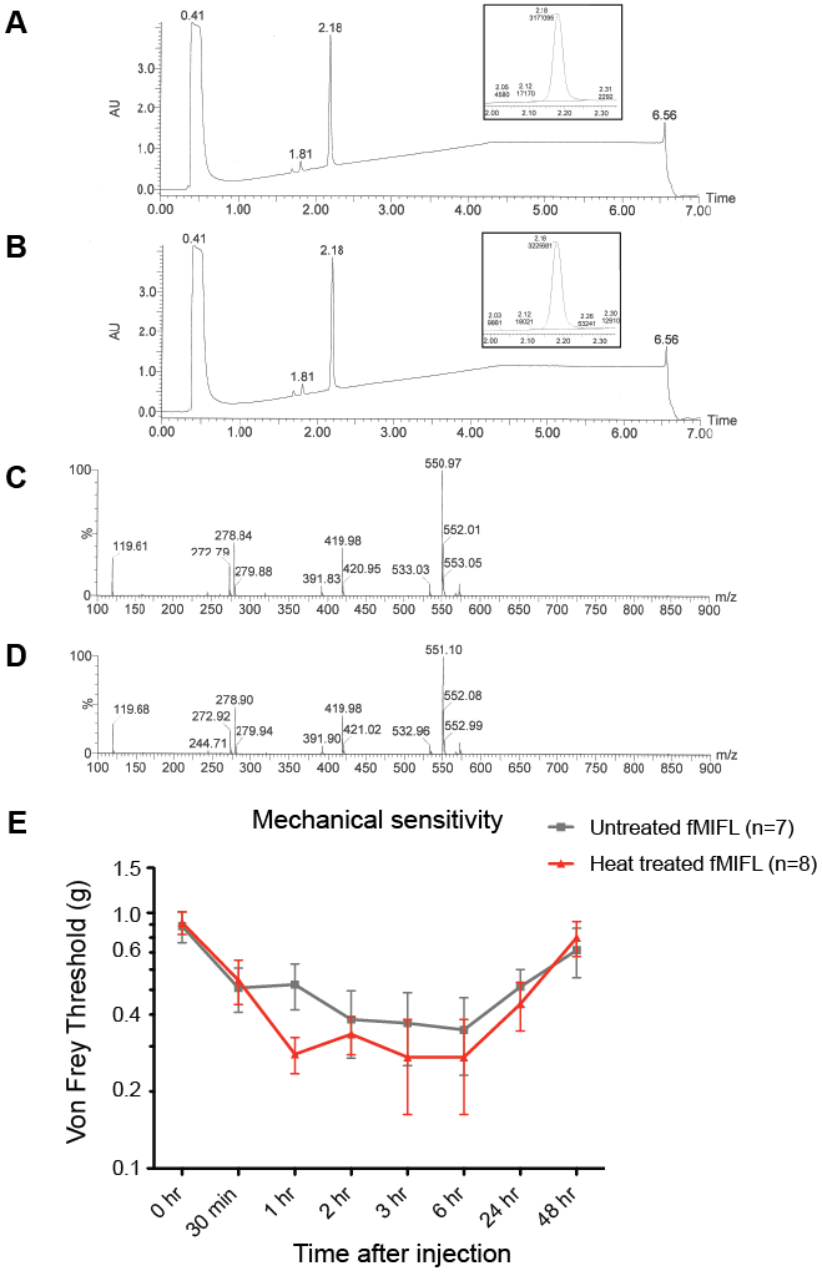

Supplementary Figure 19. Heat treatment does not alter the composition of fMIFL or its ability to induce mechanical hyperalgesia. (A-D) LC-MS analysis of fMIFL before and after heat treatment. HPLC chromatograms (λ= 220 nm) of untreated fMIFL (**A**) and after heat treatment for 100°C for 30 minutes (**B**), with the integration of the peak at 2.81 mins as the insert. The peak at 0.41 mins is the DMSO solvent peak. The peak at 2.18 mins is the peak corresponding to fMIFL with a minor unknown peak at 1.81 mins. The integration of the peak at 2.18 mins does not change after the heat treatment. ESI+ spectra of the 2.81 mins peak in untreated fMIFL (**C**) and fMIFL after heat treatment (**D**) were confirmed to be fMIFL. **(E)** Mice were injected with untreated fMIFL (n=7, 2 nmoles) or heat-treated fMIFL (n=8, 2 nmoles) show no significant differences in mechanical hypersensitivity (P=0.856, Two-way RM ANOVA).

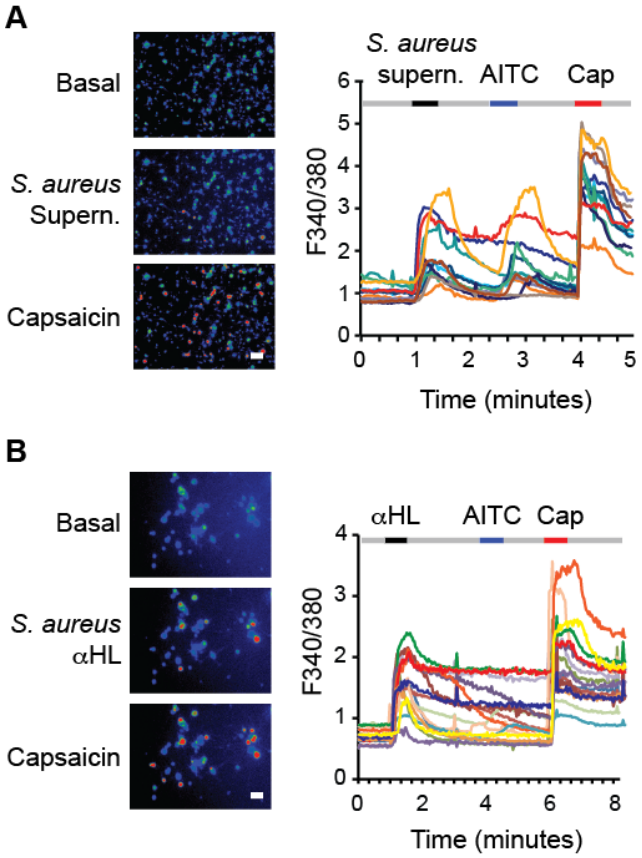

Supplementary Figure 20. *S. aureus* supernatant and the secreted toxin alpha-hemolysin (αHL) causes calcium flux in DRG neurons.
(A) *S. aureus* supernatant (5% diluted in SES), containing bacteria-secreted factors, induces calcium flux in DRG neurons, of which some respond subsequently to AITC and Capsaicin. **(B)** αHL (10 μg/mL) application induces an immediate calcium flux in subset of DRG neurons on short exposure that is able to be washed out by buffer. Some αHL responsive neurons also responded to AITC, while the majority of αHL responsive neurons also respond to capsaicin.

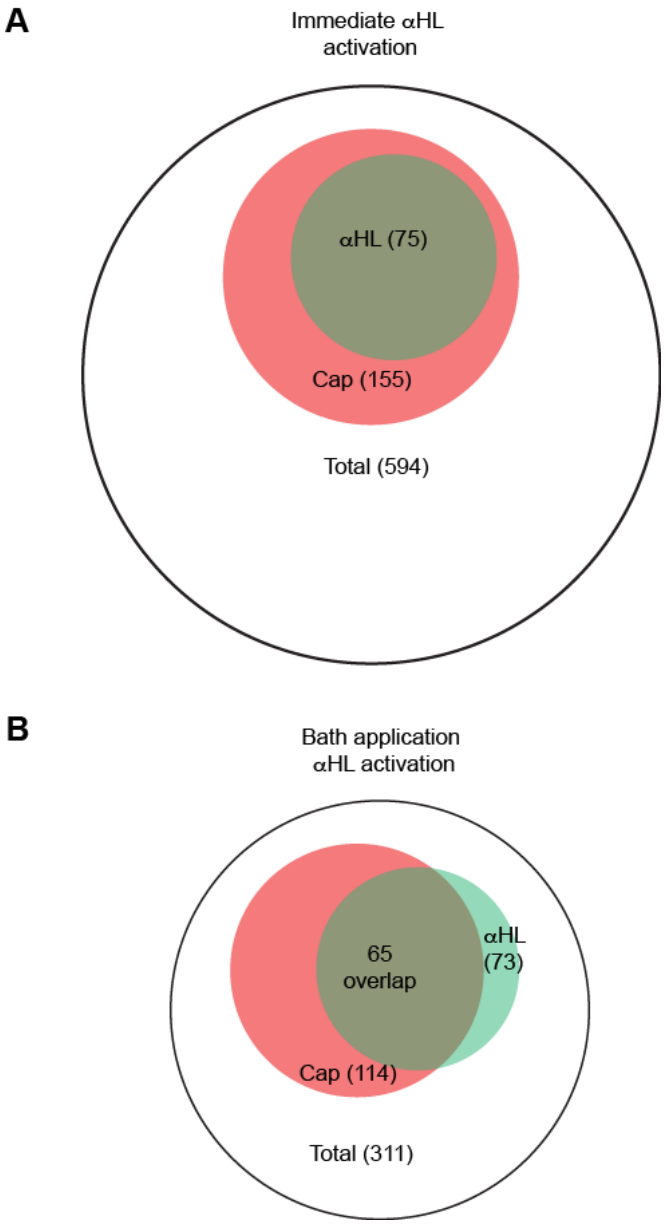

Supplementary Figure 21. αHL responsive DRG neurons are within capsaicin responsive subsets.

(A) Venn diagrams of neuronal responses to immediate application of αHL (10 μg/mL), buffer washout, and capsaicin (1 μM). All αHL responsive cells were also capsaicin responsive. **(B)** Venn diagrams showing Calcium flux responsiveness of DRG neurons from bath application of αHL (10 μg/mL). Capsaicin (1 μM) was applied after 24 minutes of αHL application. The majority of αHL responsive cells also responded to capsaicin.

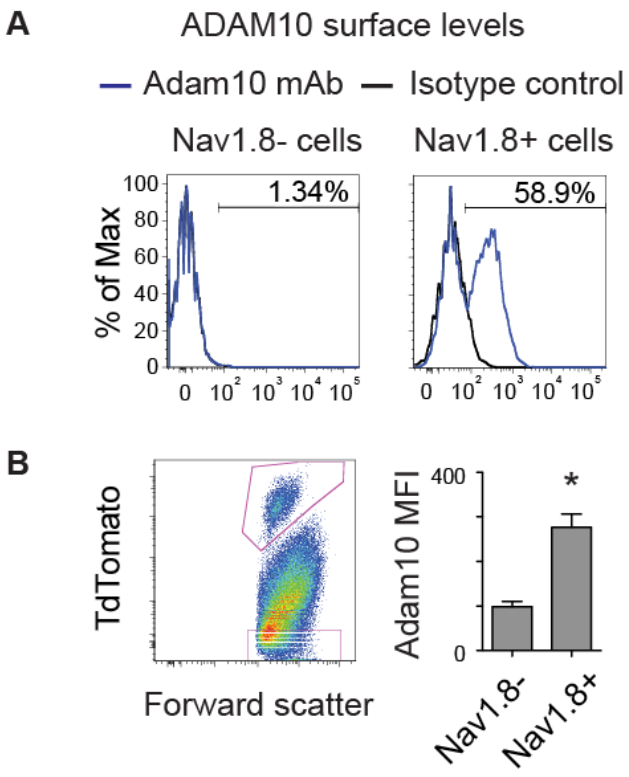

Supplementary Figure 22. ADAM10 is expressed on the surface of a subset of Nav1.8-Cre/Tdtomato+ neurons.
(A) Nav1.8-Cre/Tdtomato DRG cells stained with isotype control or anti-ADAM10 antibody analyzed by flow cytometry (see Supplemental Figure 16 for general neuron gating strategy). Histograms show 58.9% Tdtomato^{+} cells expressed surface ADAM10, while there is little staining with isotype control antibody. **(B)** Nav1.8-Cre/TdTomato^{+} cell bodies show significantly higher mean fluorescence intensity (MFI) than Tdtomato^{-} cells (flow cytometry gates for analysis on left, MFI comparison on right, n=3, *P<0.05, t-test). Error bars, mean±s.e.m.

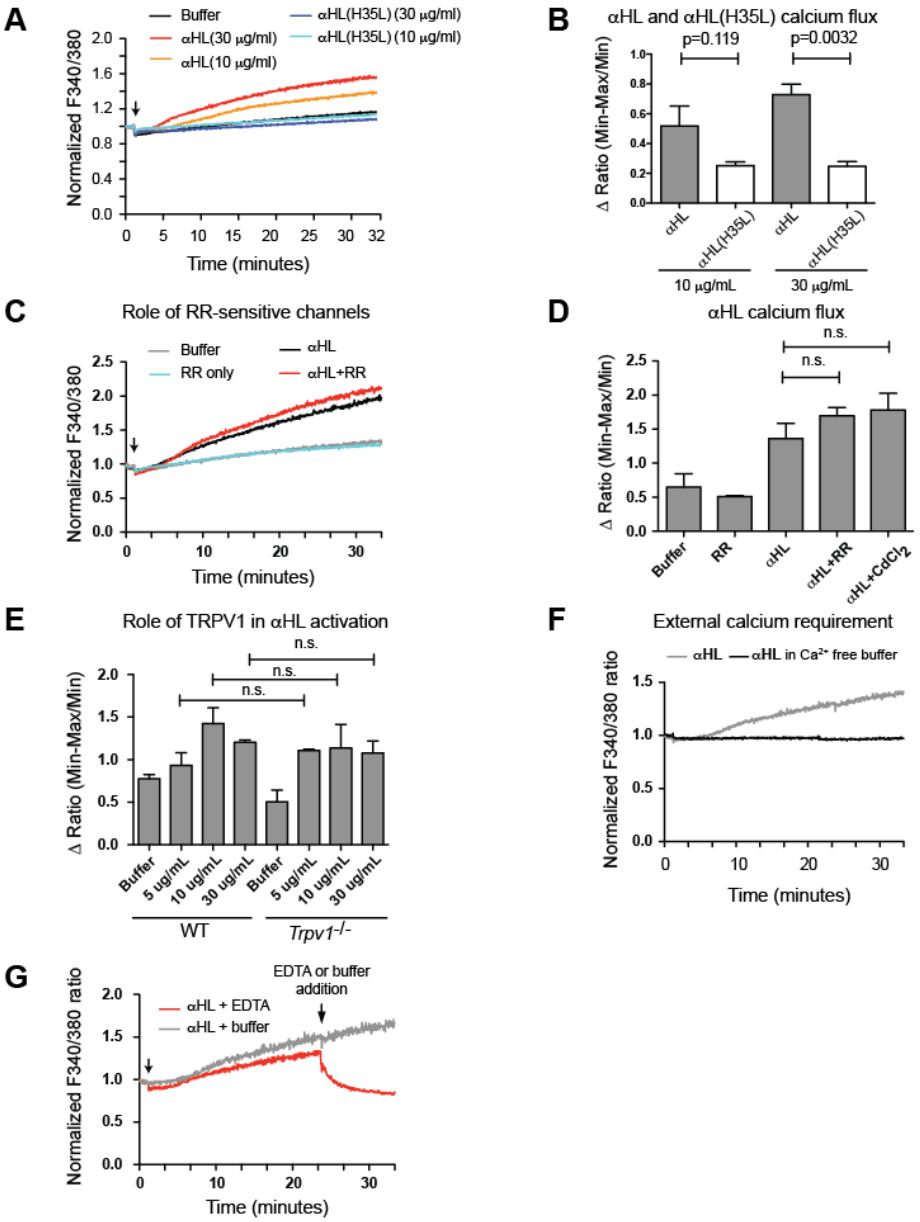

Supplementary Figure 23. Mechanism of αHL mediated calcium flux in DRG neurons. Calcium flux in DRG neurons were analyzed by whole-well Fura-2 ratiometric imaging. **(A)** Average ratiometric traces of calcium flux following application (arrow) of buffer (HBSS), αHL or mutant αHL(H35L) (10 μg/mL, 30 μg/mL). **(B)** Significantly less DRG calcium flux occurs for αHL(H35L) relative to WT αHL (P-values, t-test). **(C-D)** αHL (30 μg/mL) was applied with or without Ruthenium Red (RR, 10 uM). Normalized ratiometric traces show induction of calcium flux in the presence and absence of RR. Quantification shows no significant differences between αHL, αHL+RR (10 μM) and αHL+$CdCl_2$ (50 μM). **(E)** αHL calcium flux does not differ between WT and *Trpv1*$^{-/-}$ DRG cultures (5, 10, 30 μg/mL). **(F-G)** αHL (30 μg/mL) induced calcium flux is absent in calcium-free buffer, and addition of the chelator EDTA (5 mM) caused a decrease in αHL calcium flux. In all graphs, traces are average of triplicate wells; arrows show time of ligand application. P-values, t-test. Error bars, mean±s.e.m.

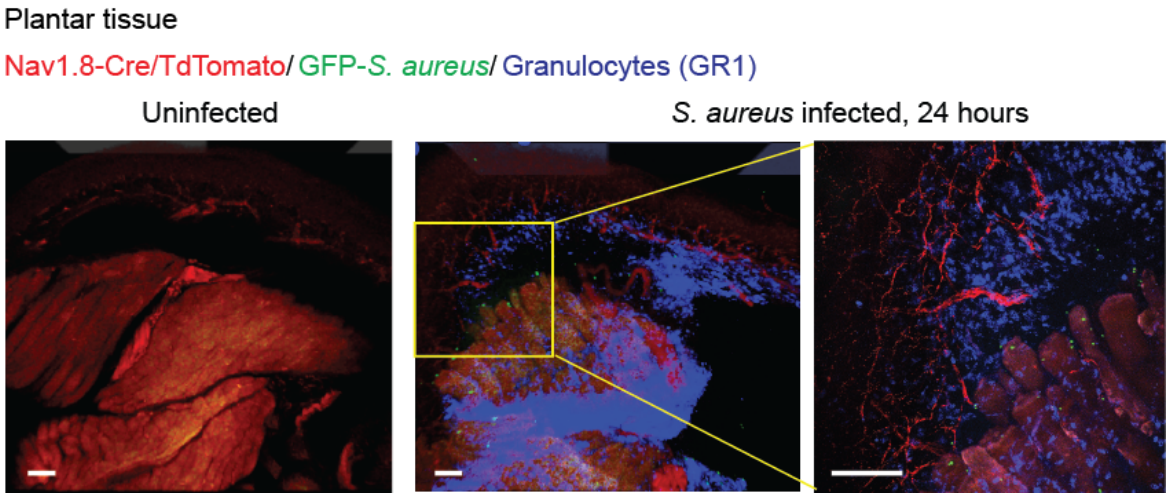

Supplementary Figure 24. Gr1$^+$ cells are found in close proximity with nociceptor nerve fibres in *S. aureus* infected plantar tissues.
Nav1.8-Cre/TdTomato mice were infected with GFP-LAC/USA300, paw tissue collected 24 h post-infection, fixed and cryosectioned. Sections were stained with anti-GR1, followed by Alexa 647 anti-Rat IgG. Confocal microscopy shows close apposition of GR1$^+$ granulocytes (blue, which includes neutrophils and monocytes) with Nav1.8-Cre/TdTomato$^+$ nociceptor nerve fibres (red) at a time-point with fewer bacteria (green). Scale bars, 100 μm.

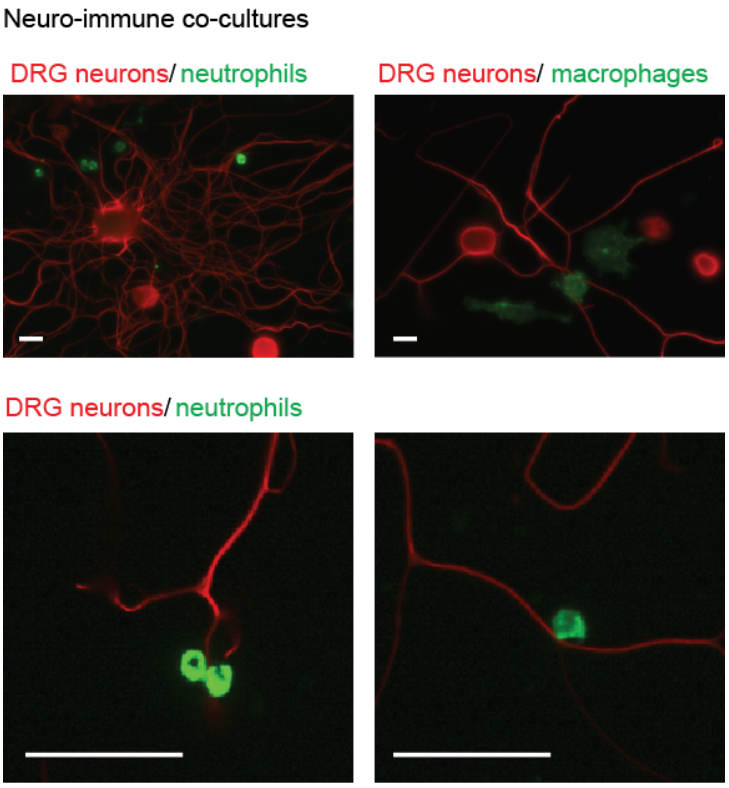

Supplementary Figure 25. Neutrophils and macrophages localize in proximity with neurites in DRG neuron co-cultures.
DRG neurons were co-cultured with bone marrow-isolated neutrophils (top left panel) or bone marrow-derived macrophages (top right panel) for 16 h *in vitro*. Higher magnification images of neutrophil-neuron co-cultures are shown in lower panels. Fixed co-cultures were stained with mouse anti-βIII-tubulin and rat anti-CD11b, followed by Alexa 488 goat anti-mouse IgG (green) and Alexa 568 goat anti-rat IgG (red). Imaging by epifluorescence microscopy. Scale bars, 10 μm.

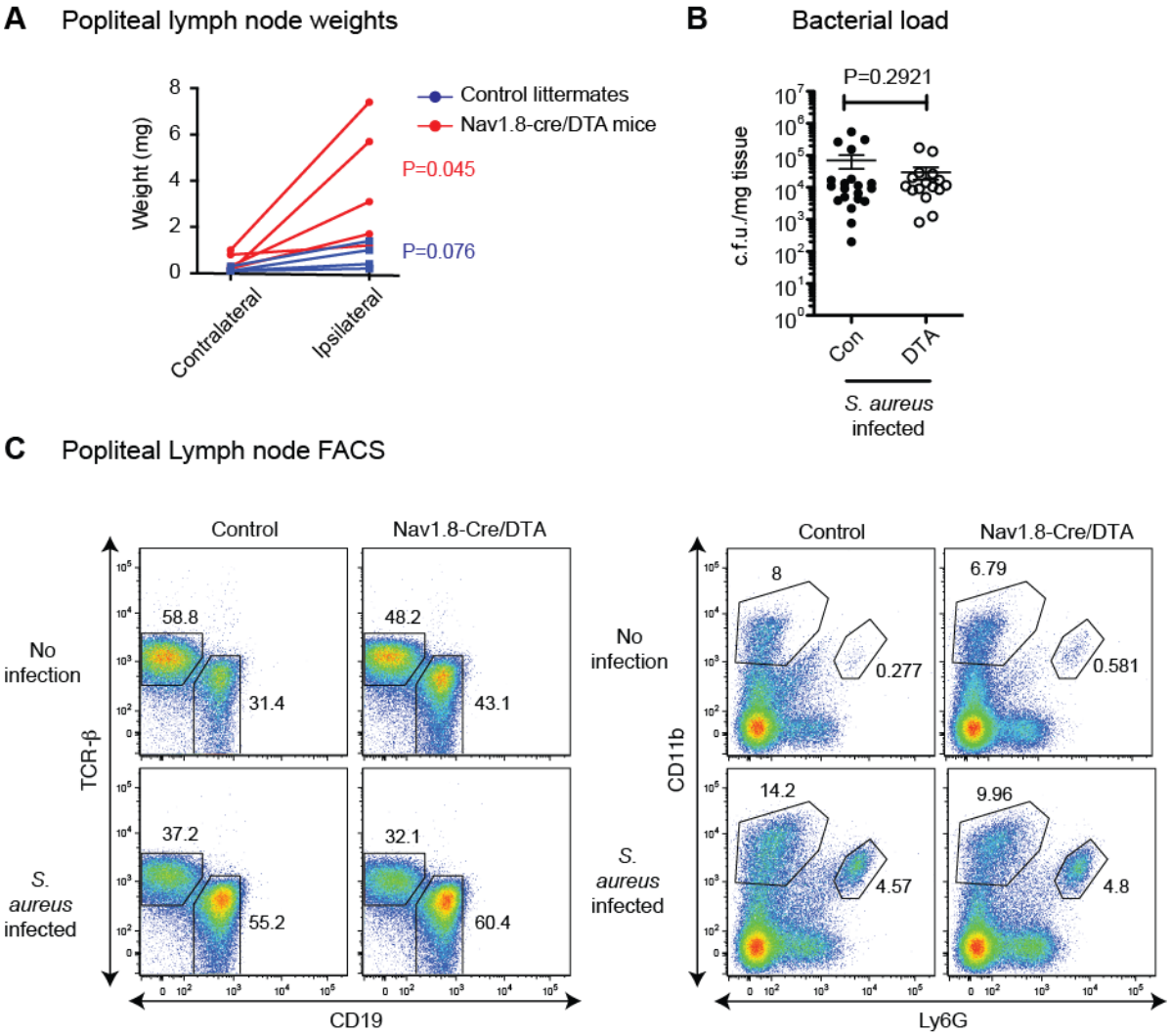

Supplementary Figure 26. Popliteal lymph node weight, bacterial load, and lymph node FACS in mice post-*S. aureus* infection. Nav1.8-Cre/DTA and control littermates infected with *S. aureus* ($5x10^6$ c.f.u.) were analyzed 24 h later. **(A)** Nav1.8-Cre/DTA mice (red) show significant differences between contralateral and ipsilateral draining popliteal lymph node weights following infection but not controls (blue) (p-values, unpaired t-test). **(B)** Bacterial load in infected tissues did not differ significantly between Nav1.8-Cre/DTA, control littermates. P-value, t-test. Error bars, mean±s.e.m. **(C)** Representative flow cytometry of popliteal lymph nodes from uninfected and infected Nav1.8-Cre/DTA or control littermates. Cells were stained with a combination of TCR-β, CD19, CD11b, Ly6G, Ly6C antibodies. Shown are representative gates for T cells ($TCR\beta^+CD19^-$), B cells ($TCR\beta^-CD19^+$), neutrophils ($CD11b^+Ly6G^+$) and myeloid cells that are not neutrophils ($CD11b^+Ly6G^-$). These data in combination with cell counts by hemocytometer were used to calculate specific numbers of lymph node subsets. We found that while overall cellularity increased in Nav1.8-Cre/DTA mice following infection, no particular lymphoid or myeloid cell-type showed dramatic proportional changes, but rather there was a general increase in T, B, and monocyte/macrophage populations (Fig. 5e).

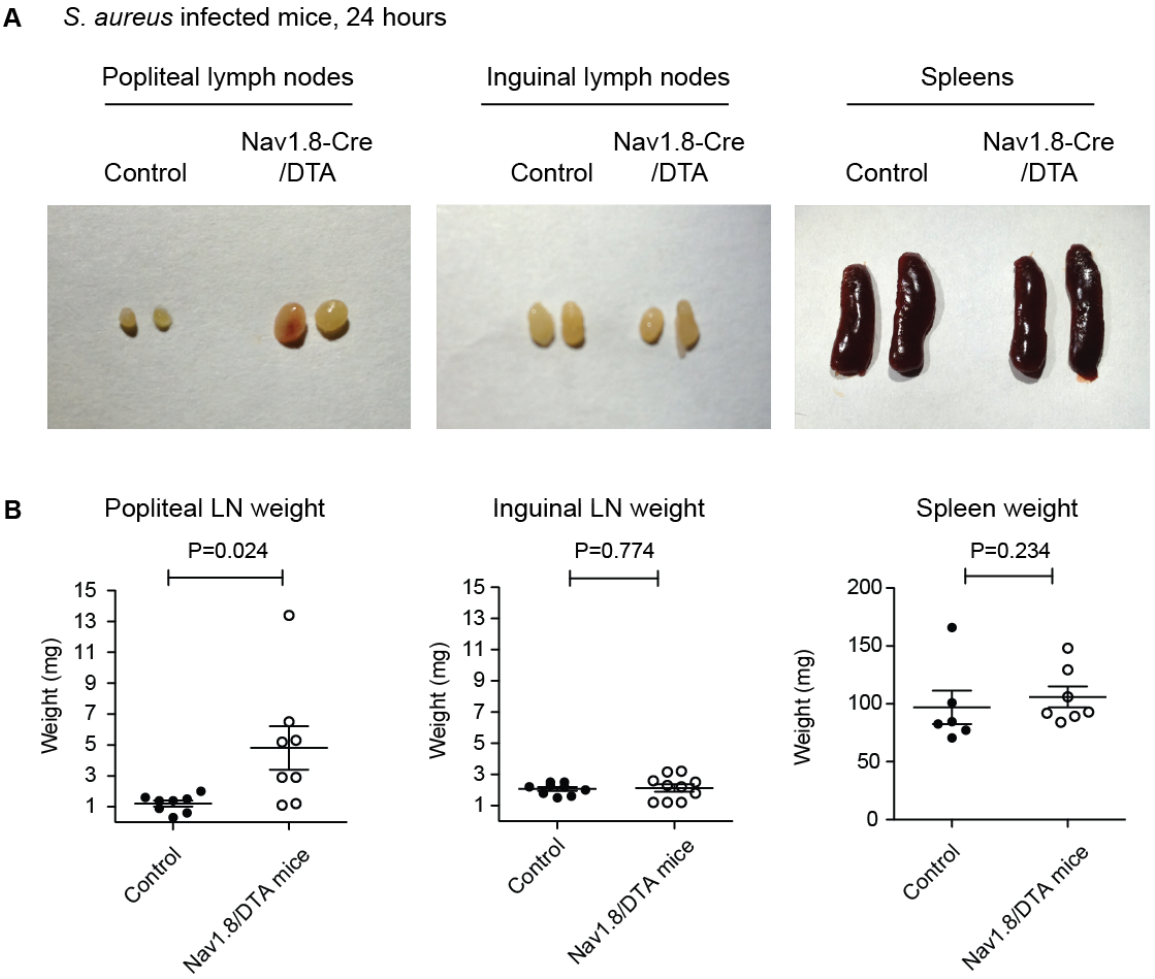

Supplementary Figure 27. Draining popliteal but not inguinal lymph nodes or spleens differ in size and weight following *S. aureus* infection of Nav1.8-Cre/DTA and control littermates.

(A) Representative images of ipsilateral popliteal lymph nodes, inguinal lymph nodes, and spleens from *S. aureus* infected animals. **(B)** Statistical comparison of weights of draining popliteal lymph nodes, inguinal lymph nodes, and spleens from infected control littermate and Nav1.8-Cre/DTA mice. P-values, t-test. Error bars, mean±s.e.m.

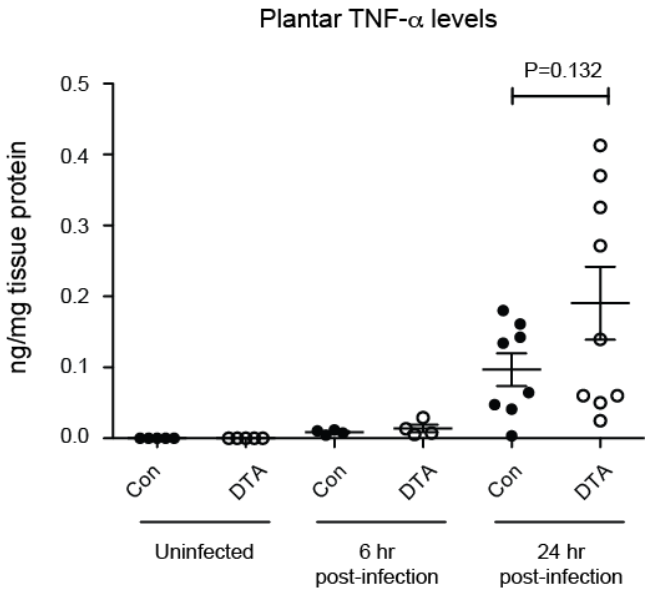

Supplementary Figure 28. Plantar TNF-α levels increase in Nav1.8-Cre/DTA mice following infection.

Plantar tissue was homogenized and analyzed for levels of TNF-α (normalized to total protein in tissue as measured by BCA assay) from Nav1.8-Cre/DTA and control mice either uninfected, infected for 6 h or for 24 h with *S. aureus* ($5x10^6$ c.f.u.) Individual mice are shown as data-points at each time-point. P-value, t-test. Error bars, mean±s.e.m.

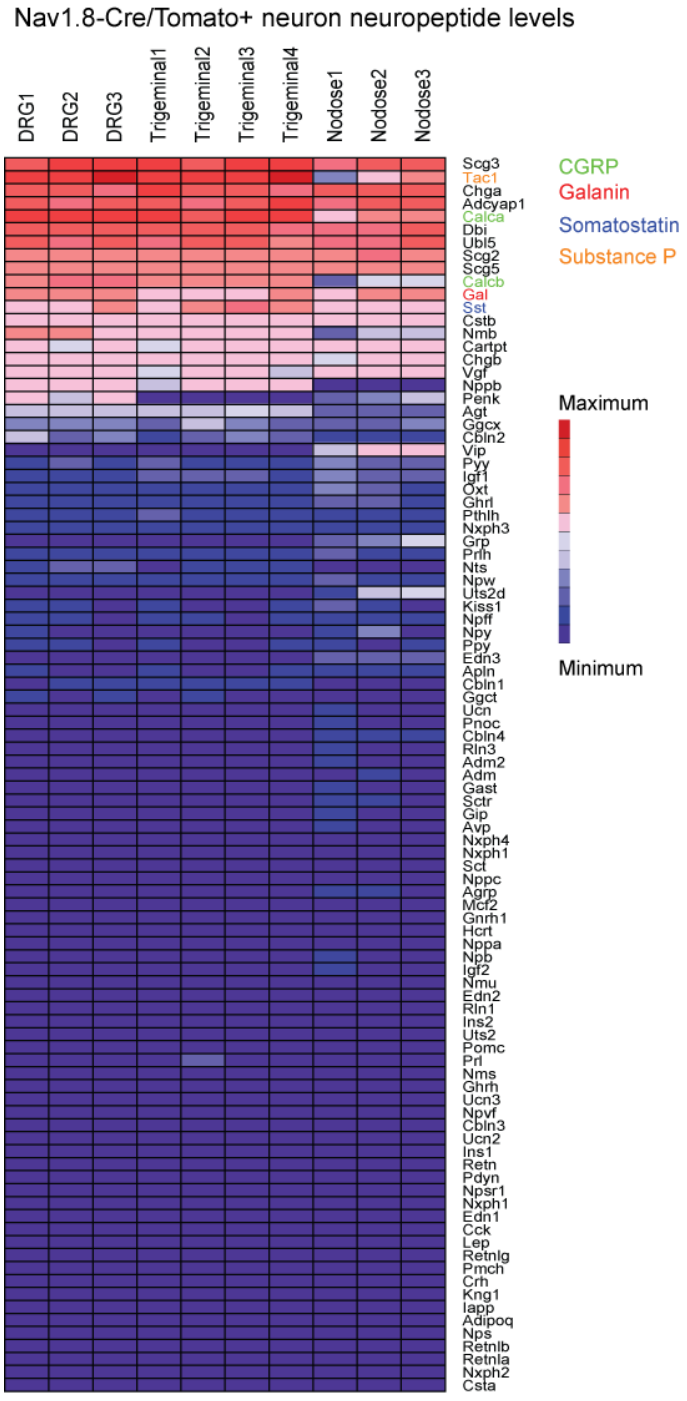

Supplementary Figure 29. Neuropeptide gene expression levels in Nav1.8-Cre/Tomato$^+$ DRG, trigeminal and nodose ganglion neurons. Nav1.8-Cre/Tomato$^+$ nociceptors were purified from DRG, trigeminal, and nodose ganglia, RNA extracted and subjected to microarray analysis. A list of neuropeptides was compiled (www.neuropeptides.nl), and corresponding average gene expression levels across all nociceptor types were ranked from maximum to minimum by average expression, and represented as a heat-map. Genes encoding CGRP (green), galanin (red), somatostatin (blue), and substance P (orange) are highlighted.

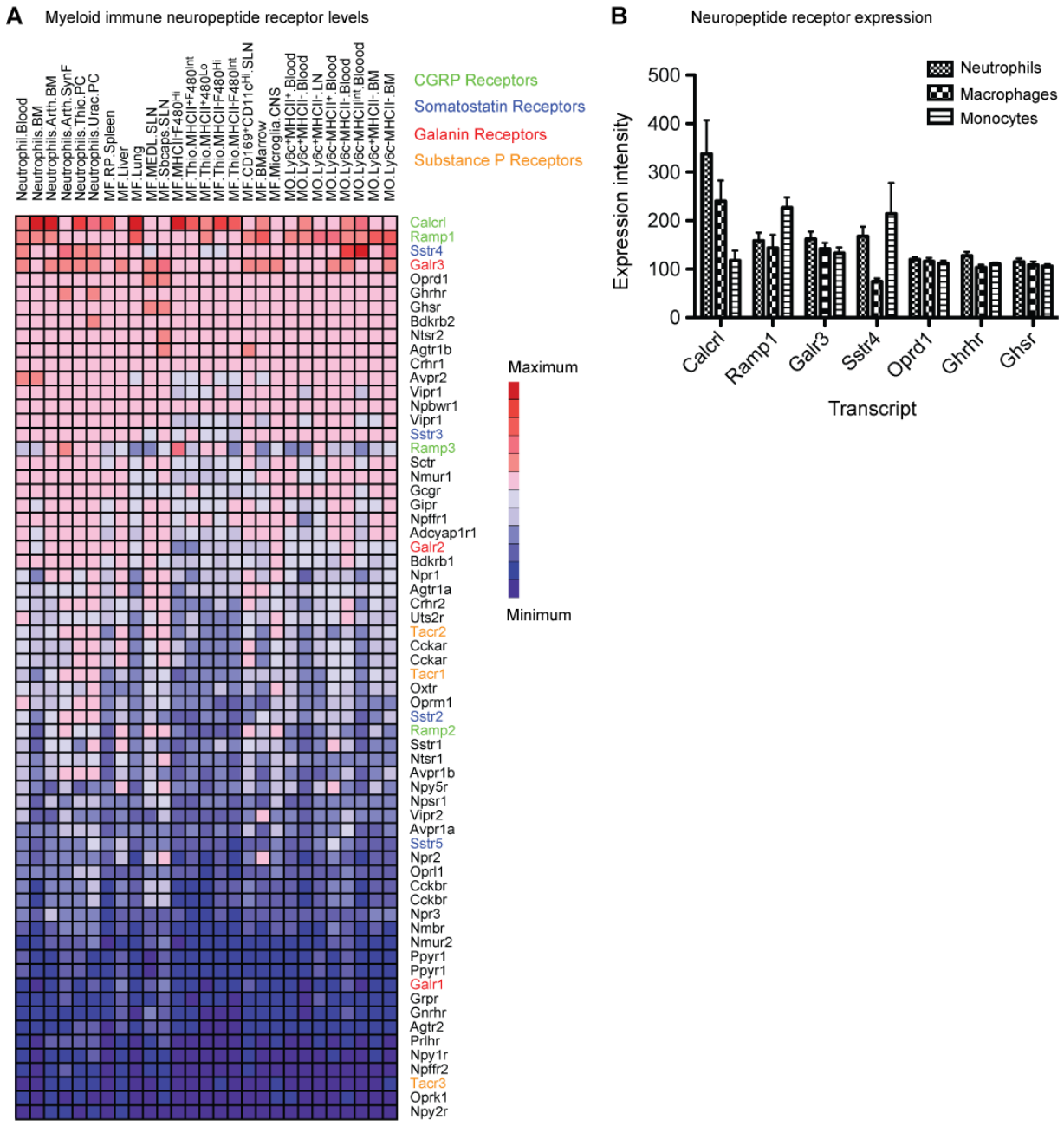

Supplementary Figure 30. Neuropeptide receptor gene expression levels in neutrophil, monocyte, and macrophage immune cell subsets. **(A)** Microarray datasets for different neutrophil, monocyte, macrophage subsets (names shown) were analyzed for average neuropeptide receptor gene expression levels, which were ranked from maximum to minimum and represented as a heat-map. Genes encoding receptors for CGRP (green), galanin (red), somatostatin (blue), and substance P (orange) are highlighted. **(B)** The top 7 neuropeptide receptors in myeloid immune cells as shown on the heat-map are plotted among neutrophil subsets, macrophage subsets, and monocyte subsets. Calcrl and Ramp1 bind CGRP, Galr3 binds galanin, and Sstr4 binds somatostatin. Error bars, mean±s.e.m.

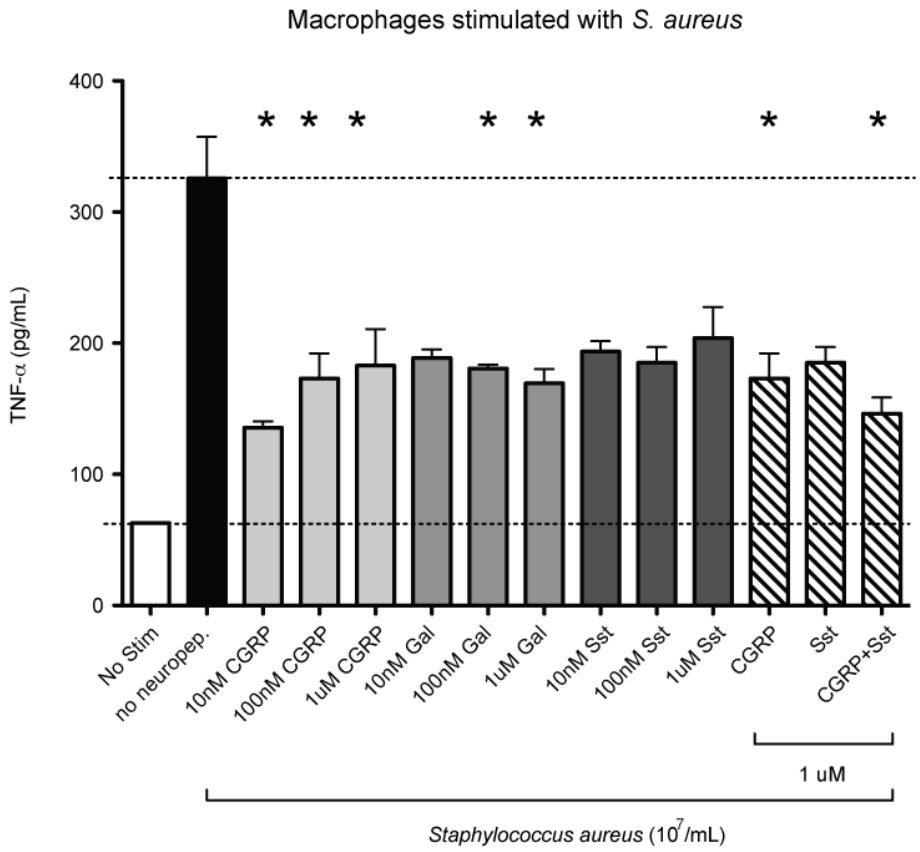

Supplementary Figure 31. CGRP, Galanin, and Somatostatin modulate macrophage TNF-α release in response to *S. aureus* stimulation.
Increasing concentrations of CGRP, Galanin (Gal) or Somatostatin (Sst) or combined CGRP and Sst were added in conjunction with hk-*S. aureus* (10^7 c.f.u./mL) to cultured bone marrow derived macrophages for 16 h at 37°C. Supernatants were collected and analyzed for TNF-α by ELISA. (*P<0.05, t-test compared to macrophages stimulated with hk-*S. aureus* in the absence of neuropeptides, performed in biological triplicates). Note: Some data are presented in Fig. 6, and this figure contains the full-range of concentrations tested. Error bars, mean±s.e.m.

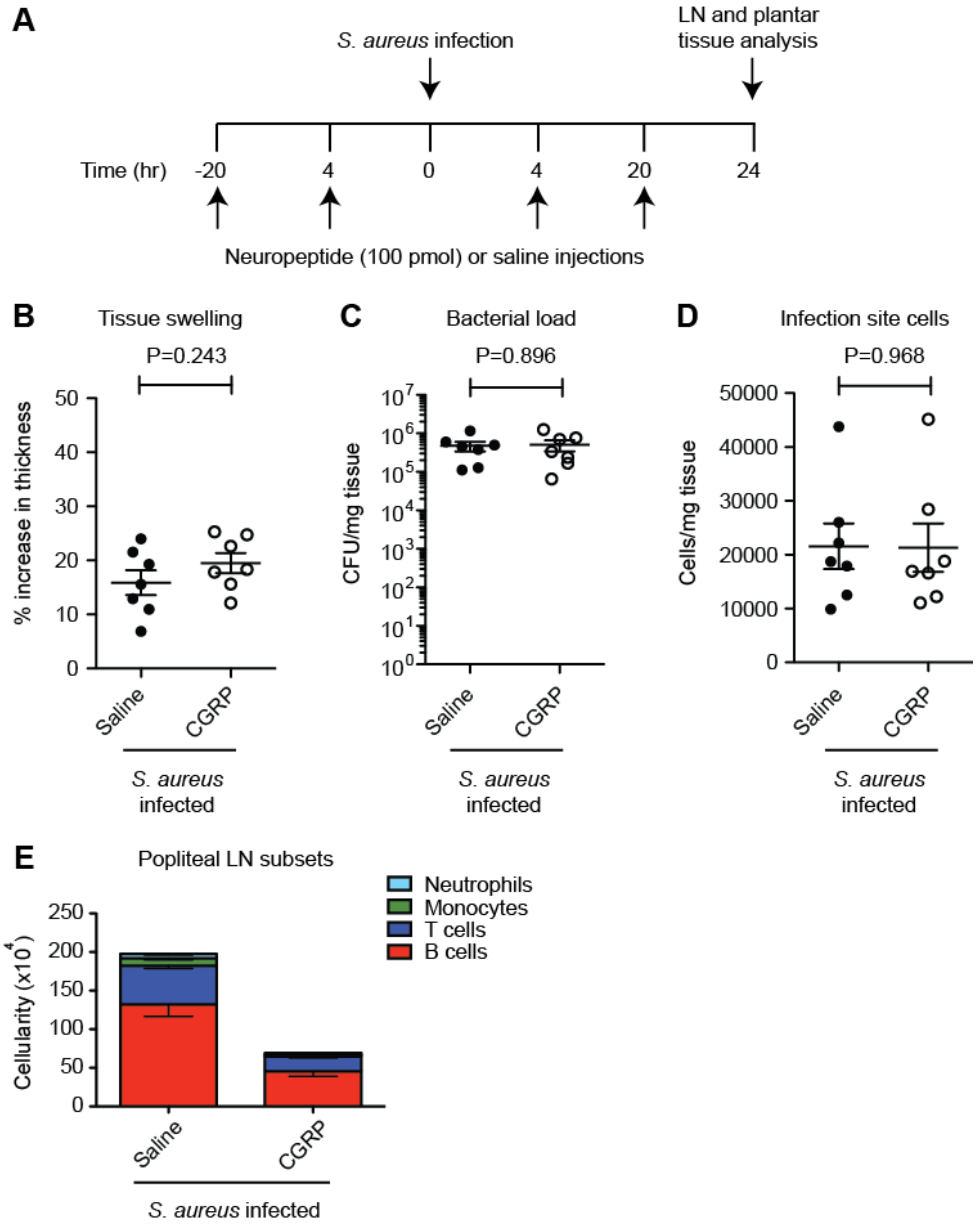

Supplementary Figure 32. CGRP injection does not affect *S. aureus* induced plantar inflammation but decreases lymphadenopathy.
(A) CGRP injection and *S. aureus* infection experimental scheme, followed by tissue collected and analysis 24 h post-infection. **(B)** CGRP injection did not affect tissue swelling as measured by % increase in thickness from baseline following infection (P-value, t-test). **(C)** Bacterial load at the infection site was not affected by CGRP injection (P-value, t-test). **(D)** Plantar tissue was analyzed for infection site cell numbers, which increase following infection, which include neutrophils and monocytes (P-value, t-test). **(E)** Draining popliteal lymph node cells counted for total cellularity showed significant decreases following CGRP injection (Fig. 6e). Here, these cells were analyzed by flow cytometry for specific immune subsets, including neutrophil, monocyte, T cells, and B cells. Error bars, mean±s.e.m.

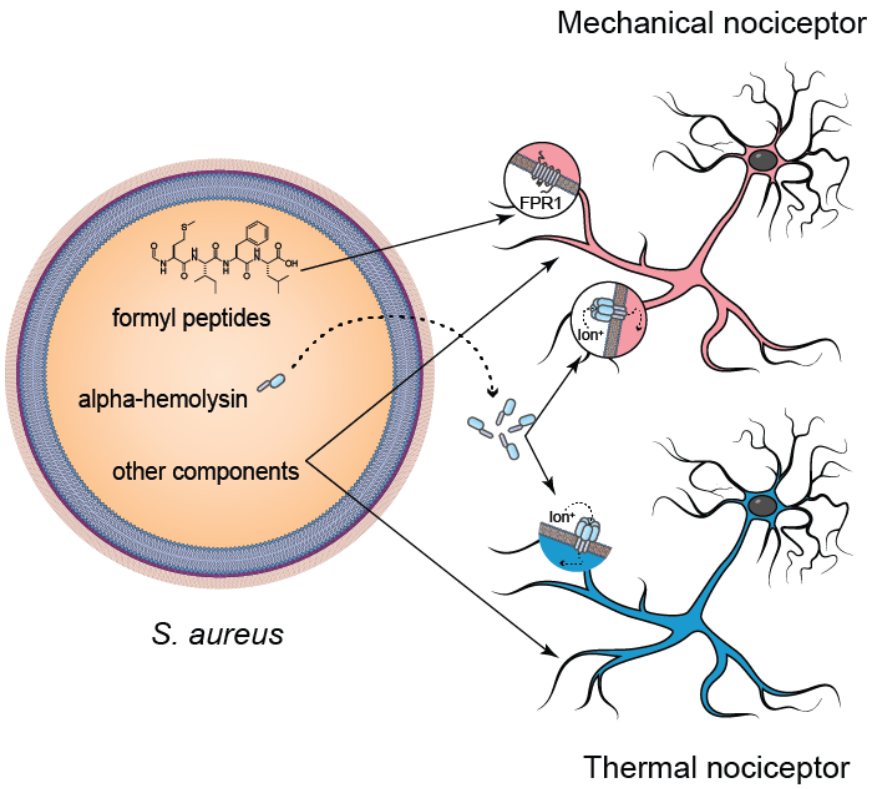

Supplementary Figure 33. Bacteria directly activate nociceptor neurons through distinct mechanisms.
Bacteria directly activate nociceptors through several distinct mechanisms: 1) N-formylated peptides, heat-stable components found in bacteria, activate FPR1 on a subset of nociceptor neurons that mediate mechanical but not heat hyperalgesia. 2) αHL, a heat-sensitive pore-forming toxin secreted by *S. aureus*, binds to nociceptor cell membranes, and oligomerizes to form pores allowing ionic entry and depolarization. This is sufficient to induce mechanical and thermal hyperalgesia. 3) Other unidentified molecular components from bacteria likely activate nociceptors that mediate mechanical and thermal hypersensitivity.